A genome-wide resource for the analysis of protein localisation in *Drosophila*

Mihail Sarov[1], Christiane Barz[2], Helena Jambor[1], Marco Y. Hein[3], Christopher Schmied[1], Dana Suchold[1], Bettina Stender[2], Stephan Janosch[1], Vinay K.J. Vikas[4], R.T. Krishnan[4], K. Aishwarya[4], Irene R. S. Ferreira[2], Radoslaw K. Ejsmont[1], Katja Finkl[2], Susanne Hasse[1], Philipp Kämpfer[5], Nicole Plewka[2], Elisabeth Vinis[1], Siegfried Schloissnig[5], Elisabeth Knust[1], Volker Hartenstein[6], Matthias Mann[3], Mani Ramaswami[7], K.VijayRaghavan[4], Pavel Tomancak[1] and Frank Schnorrer[2]

[1] Max Planck Institute of Cell Biology and Genetics, Pfotenhauerstr. 108, 01307 Dresden, Germany

[2] Muscle Dynamics Group, Max Planck Institute of Biochemistry, Am Klopferspitz 18, 82152 Martinsried, Germany

[3] Department of Proteomics and Signal Transduction, Max Planck Institute of Biochemistry, Am Klopferspitz 18, 82152 Martinsried, Germany

[4] Centre for Cellular and Molecular Platforms, National Centre for Biological Sciences, Tata Institute of Fundamental Research, Bald Bellary Road, Bangalore 560065, India

[5] Heidelberg Institute of Theoretical Studies, Schloss-Wolfsbrunnenweg 35, 69118 Heidelberg, Germany

[6] Department of Molecular Cell and Developmental Biology, University of California, Los Angeles, 610 Charles E. Young Drive, 5009 Terasaki Life Sciences Building, Los Angeles, CA 90095, USA

[7] Institute of Neuroscience, Trinity College Dublin, Dublin 2, Ireland

correspondence should be addressed to:

sarov@mpi-cbg.de

tomancak@mpi-cbg.de

schnorrer@biochem.mpg.de

Abstract

The *Drosophila* genome contains >13,000 protein coding genes, the majority of which remain poorly investigated. Important reasons include the lack of antibodies or reporter constructs to visualise these proteins. Here we present a genome-wide fosmid library of 10,000 GFP-tagged clones, comprising tagged genes and most of their regulatory information. For 880 tagged proteins we created transgenic lines and for a total of 207 lines we assessed protein expression and localisation in ovaries, embryos, pupae or adults by stainings and live imaging approaches. Importantly, we visualised many proteins at endogenous expression levels and found a large fraction of them localising to subcellular compartments. By applying genetic complementation tests we estimate that about two-thirds of the tagged proteins are functional. Moreover, these tagged proteins enable interaction proteomics from developing pupae and adult flies. Taken together, this resource will boost systematic analysis of protein expression and localisation in various cellular and developmental contexts.

Impact statement

We provide a large-scale transgenic resource, which enables live imaging, subcellular localisation and interaction proteomics of selected gene products at all stages of *Drosophila* development.

Introduction

With the complete sequencing of the *Drosophila* genome (Adams et al., 2000) genome-wide approaches have been increasingly complementing the traditional single gene, single mutant studies. This is exemplified by the generation of a genome-wide transgenic RNAi library (Dietzl et al., 2007) to systematically assess gene function in the fly or by the documentation of the entire developmental transcriptome during all stages of the fly's life cycle by mRNA sequencing (Graveley et al., 2011). Furthermore, expression patterns were collected for many genes during *Drosophila* embryogenesis by systematic mRNA *in situ* hybridisation studies in different tissues (Hammonds et al., 2013; Tomancak et al., 2002; 2007). Particularly for transcription factors (TFs) these studies revealed complex and dynamic mRNA expression patterns in multiple primordia and organs during development (Hammonds et al., 2013), supposedly driven by specific, modular enhancer elements (Kvon et al., 2014). Furthermore, many mRNAs are not only dynamically expressed but also subcellularly localised during *Drosophila* oogenesis (Jambor et al., 2015) and early embryogenesis (Lécuyer et al., 2007). Together, these large-scale studies at the RNA level suggest that the activity of many genes is highly regulated in different tissues during development. Since the gene function is mediated by the encoded protein(s), the majority of proteins should display particular expression and subcellular localisation patterns that correlate with their function.

However, a lack of specific antibodies or live visualisation probes thus far hampered the systematic survey of protein expression and localisation patterns in various developmental and physiological contexts in *Drosophila*. Specific antibodies are only available for about 450 *Drosophila* proteins (Nagarkar-Jaiswal et al., 2015), and the versatile epitope-tagged UAS-based overexpression collection that recently became available (Bischof et al., 2013; Schertel et al., 2015) is not suited to study protein

distribution at endogenous expression levels. Collections of knock-in constructs are either limited to specific types of proteins (Dunst et al., 2015) or rely on inherently random genetic approaches, such as the large-scale protein-trap screens or the recently developed MiMIC (Minos Mediated Insertion Cassette) technology (Venken et al., 2011). The classical protein-trap screens are biased for highly expressed genes, and altogether recovered protein traps in 514 genes (Buszczak et al., 2007; Lowe et al., 2014; Morin et al., 2001; Quiñones-Coello et al., 2007). The very large scale MiMIC screen isolated insertions in the coding region of 1,862 genes, 200 of which have been converted into GFP-traps available to the community (Nagarkar-Jaiswal et al., 2015). Both approaches rely on transposons to mediate cassette insertion and require integration into an intron surrounded by coding exons for successful protein tagging. Thus, about 3,000 proteins, whose ORF is encoded within a single exon, cannot be tagged by these approaches (analysis performed using custom Perl script available here: https://github.com/tomancak/intronless_CDS_analysis). Together, this creates a significant bias towards trapping a particular subset of the more than 13,000 protein coding genes in the fly genome.

Hence, the *Drosophila* community would profit from a resource that enables truly systematic protein visualisation at all developmental stages for all protein coding genes, while preserving the endogenous expression pattern of the tagged protein. One strategy to generate a comprehensive resource of tagged proteins is to tag large genomic clones by recombineering approaches in bacteria and transfer the resulting tagged clones into animals as third copy reporter allele as was previously done in *C. elegans* (Sarov et al., 2012). The third copy reporter allele approach was used successfully in *Drosophila* with large genomic BAC or fosmid clones derived from the fly genome. In *Drosophila* it is possible to insert this tagged copy of the gene as a transgene at a defined position into the fly genome

97 (Venken et al., 2006). It has been shown that such a transgene recapitulates the endogenous
98 expression pattern of the gene in flies and thus likely provides a tagged functional copy of
99 the gene (Ejsmont et al., 2009; Venken et al., 2009).

100 Here, we introduce a comprehensive genome-wide library of almost 10,000 C-
101 terminally tagged proteins within genomic fosmid constructs. For 880 constructs, covering
102 826 different genes we generated transgenic lines, 765 of which had not been tagged by
103 previous genetic trapping projects. Rescue experiments using a subset of lines suggest that
104 about two thirds of the tagged proteins are functional. We characterised the localisation
105 patterns for more than 200 tagged proteins at various developmental stages from ovaries to
106 adults by immunohistochemistry and by live imaging. This identified valuable markers for
107 various tissues and subcellular compartments, many of which are detectable *in vivo* by live
108 imaging. Together, this shows the wide range of possible applications and the potential
109 impact this publically available resource will have on *Drosophila* research and beyond.

Results

Our goal was to generate a comprehensive resource that allows the investigation of protein localisation and physical interactions for any fly protein of interest through a robust, generic tagging pipeline in bacteria, which is followed by a large-scale transgenesis approach (**Figure 1A**). We based our strategy on a *Drosophila melanogaster* FlyFos library of genomic fosmid clones, with an average size of 36 kb, which covers most *Drosophila* genes (Ejsmont et al., 2009). Our two-step tagging strategy first inserts a generic 'pre-tag' at the C-terminus of the protein, which is then replaced by any tag of choice at the second tagging step, for example with a superfolder-GFP (sGFP) tag to generate the sGFP TransgeneOme clone library. These tagged clones are injected into fly embryos to generate transgenic fly-TransgeneOme (fTRG) lines, which can be used for multiple *in vivo* applications. (**Figure 1A**).

sGFP TransgeneOme – a genome-wide tagged FlyFos clone library

We aimed to tag all protein coding genes at the C-terminus of the protein, because a large number of regulatory elements reside within or overlap with the start of genes, including alternative promoters, enhancer elements, nucleosome positioning sequences, etc. These are more likely to be affected by a tag insertion directly after the start codon. Signal sequences would also be compromised by an inserted tag after the start codon. This is in agreement with a recently published dataset favouring C-terminal compared to N-terminal tagging (Stadler et al., 2013). Additionally, the C-termini in the gene models are generally better supported by experimental data than the N-termini due to an historical bias for 3'-end sequencing of ESTs. Thus, C-terminal tagging is more likely to result in a functional tagged protein than N-terminal tagging, although we are aware of the fact that some proteins will be likely inactivated by addition of a tag to the C-terminus. Moreover, only

about 1,400 protein coding genes contain alternative C-termini, resulting in all protein isoforms labelled by C-terminal tagging for almost 90 % of all protein coding genes (analysis performed using custom Perl script available here: https://github.com/tomancak/alternative_CDS_ends).

In a series of pilot experiments we tested the functionality of several tagging cassettes with specific properties on a number of proteins (**Figure 1-figure supplement 1, Table 1**). For the genome-wide resource we applied a two-step tagging strategy, whereby we first inserted a non-functional 'pre-tagging' cassette consisting of a simple bacterial selection marker, which is flanked with linker sequences present in all of our tagging cassettes. This strategy enables a very efficient replacement of the 'pre-tag' by any tag of interest using homologous recombination mediated cassette exchange in bacteria (Hofemeister et al., 2011). As fluorescent proteins and affinity tags with improved properties are continuously being developed, specific clones or the entire resource can be easily re-fitted to any new tagging cassette. For the genome-scale resource we selected a tagging cassette suitable for protein localisation and complex purification studies, consisting of the 2xTY1 tag as a flexible linker, the superfolder GFP coding sequence (Pédelacq et al., 2005), the V5 tag, followed by specific protease cleavage sites (for the PreScission- and TEV-proteases), the biotin ligase recognition peptide (BLRP) tag allowing for specific *in vivo* or *in vitro* biotinylation (Deal and Henikoff, 2010; Vernes, 2014), and the 3xFLAG tag (**Figure 1-figure supplement 1**).

Of the 13,937 protein coding genes in the dmel5.43 genome assembly, 11,787 genes (84.6 %) were covered by a suitable fosmid from the original FlyFos library (Ejsmont et al., 2009), extending at least 2.5 kb upstream and 2.5 kb downstream of the annotated gene model. For picking clones, designing oligonucleotides for recombineering, and for tracking all steps of the transgene engineering process, as well as for providing

160 access to all construct sequences and validation data we used the previously developed
161 TransgeneOme database (Sarov et al., 2012), which is available online
162 (https://transgeneome.mpi-cbg.de).

163 For high-throughput tagging of the *Drosophila* FlyFos clones, we developed an
164 improved version of our previously applied high-throughput, 96-well format liquid culture
165 recombineering pipeline (Ejsmont et al., 2011; Sarov et al., 2012) and we applied it to
166 create a single tagged construct for each gene covered by a suitable fosmid. The high
167 efficiency of recombineering in *E. coli* allowed for multi-step DNA engineering in 96-well
168 format liquid cultures with single clone selection only at the last step. The pipeline consists
169 of five steps (**Figure 1B**). First, the pRedFlp helper plasmid containing all genes required
170 for homologous recombination and the Flippase-recombinase (under L-rhamnose and
171 tetracycline control, respectively) was introduced into *E. coli* by electroporation. Second,
172 the 'pre-tagging' cassette containing a bacterial antibiotic resistance gene was inserted by
173 homologous recombination with gene-specific homology arms of 50 base pairs. Third, the
174 sGFP-V5-BLRP tagging cassette, including an FRT-flanked selection and counter-selection
175 cassette, was inserted to replace the 'pre-tagging' cassette. Since the linker sequences in the
176 'pre-tagging' cassette are identical to the tagging cassette, the tagging cassette was simply
177 excised from a plasmid by restriction digest and no PCR amplification was required. This
178 strongly reduced the risk of PCR-induced mutations in the tagging cassette. Fourth, the
179 selection marker was excised by the induction of Flippase expression. Fifth, the helper
180 plasmid was removed by suppression of its temperature sensitive replication at 37 ºC
181 (Meacock and Cohen, 1980) and single clones were isolated from each well by plating on
182 selective solid agar plates.

183 All five steps of the engineering pipeline were highly efficient (between 95.8 and
184 99.7 %), resulting in an overall efficiency of 93.6 % or 10,995 growing cultures (**Figure**

185 **1B**). To validate the sequence of the engineered clones we developed a new next-
186 generation-sequencing (NGS)-based approach (**Figure 1C**). In short, we pooled single
187 clones from all 96-well plates into 8 rows and 12 columns pools, prepared barcoded mate
188 pair libraries from each pool, and sequenced them using a Illumina platform. The mate pair
189 strategy allowed us to map the otherwise common tag coding sequence to a specific clone
190 in the library and thus to verify the integrity of the tagging cassette insertion in the clones
191 with single nucleotide resolution (see Materials and Methods for details). When applied to
192 the final sGFP TransgeneOme collection we detected no mutations for 9,580 constructs
193 (87.1 %). 8,005 (72.8 %) of these clones had complete sequence coverage of the tag coding
194 sequence and thus represent the most reliable subset of the tagged library (**Figure 1C**). For
195 1,417 of the clones (12.8 %) one or more differences to the expected sequences were
196 detected. The most common differences were point mutations, which cluster almost
197 exclusively to the homology regions in the oligonucleotides used to insert the 'pre-tagging'
198 cassette. This is suggestive of errors in the oligonucleotide synthesis. Another subset of
199 point mutations clustered around the junctions between the homology arms and the rest of
200 the tagging cassette, indicating an imprecise resolving of the homology exchange reaction
201 in small subset of clones (**Figure 1D**). Finally, a small group of clones (165) still contained
202 an un-flipped selection cassette. The NGS results were confirmed by Sanger sequencing of
203 the entire tag coding sequence for a subset of constructs (**Supplementary File 1**). The
204 detailed sequencing results for all clones is available at https://transgeneome.mpi-cbg.de.
205 Taken together, the sGFP TransgeneOme and our pilot tagging experiments resulted
206 in 10,711 validated tagged clones, representing 9,993 different *Drosophila* genes. (**Table 1,**
207 **Supplementary File 1**). The clones are available from Source BioScience as *Drosophila*
208 TransgeneOme Resource (MPI-CBG)
209 (http://www.lifesciences.sourcebioscience.com/clone-products/non-

mammalian/drosophila/drosophila-transgeneome-resource-mpi-cbg/). Moreover, the 'pre-tagged' TransgeneOme library is a versatile resource for generating fosmid clones with arbitrary tags at the C-terminus of the gene models.

Fly TransgeneOme (fTRG) – a collection of fly strains with tagged fosmids transgenes

We next established a pipeline to systematically transform the tagged TransgeneOme clones into flies. To efficiently generate fly transgenic lines we injected the tagged fosmid constructs into a recipient stock carrying the attP landing site VK00033 located at 65B on the third chromosome using a transgenic *nanos*-ΦC31 source (Venken et al., 2006). For some genes positioned on the third chromosome we injected into VK00002 located on the second chromosome at 28E to simplify genetic rescue experiments. In total, we have thus far generated lines for 880 tagged constructs representing 826 different genes (**Table 1, Supplementary File 2**). These genes were partially chosen based on results of a public survey amongst the *Drosophila* community to identify genes for which there is the strongest demand for a tagged genomic transgenic line. 765 (87 %) of the newly tagged genes have not been covered by the previous protein-trap projects (**Supplementary File 2**), hence, these should be particularly useful for the fly community. From our pilot tagging experiments, we made 51 lines for the 2xTY1-sGFP-3xFLAG tag and 30 lines for the 2xTY1-T2A-sGFPnls-FLAG transcriptional reporter. The majority of the lines (799) were generated with the versatile 2xTY1-sGFP-V5-Pre-TEV-BLRP-3xFLAG tag, used for the genome-wide resource (**Figure 1-figure supplement 1, Table 1**). The collection of fly lines is called 'tagged fly TransgeneOme' (fTRG) and all 880 fTRG lines have been deposited at the VDRC stock centre for ordering (http://stockcenter.vdrc.at).

To assess whether the tagged fosmids in our transgenic library are functional, we have chosen a set of 46 well-characterised genes, mutants of which result in strong

developmental phenotypes. For most cases, we tested null or strong hypomorphic alleles for rescue of the respective phenotypes (embryonic lethality, female sterility, flightlessness, etc.) with the tagged fosmid lines. More than two-thirds of the lines (31 of 46), including tagged lines of *babo, dlg1, dl, fat, Ilk, LanB1, numb, osk, rhea, sax, smo* and *yki* rescued the mutant phenotypes (**Figure 2A**, **Table 2**), demonstrating that the majority of the tagged genes is functional. Our rescue test set is biased towards important developmental regulators; 10 of the 15 genes that did not show a rescue are transcription factors with multiple essential roles during development, such as *esg, eya, odd, sna* and *salm*. Thus, their expression is likely regulated by complex cis-regulatory regions that may not be entirely covered by the available fosmid clone; for example wing-disc enhancers are located more than 80 kb away from the transcriptional start of the *salm* gene (De Celis et al., 1999). Hence, we expect that a typical gene, which is embedded within many other genes in the middle of the fosmid clone, is more likely to be functional. Together, these data suggest that both the genome-wide tagged construct library and the transgenic fTRG library provide functional reagents that are able to substitute endogenous protein function.

Expression of fTRG lines in the ovary

To demonstrate the broad application spectrum of our fly TransgeneOme library we analysed tagged protein expression and subcellular localisation in multiple tissues at various developmental stages. Germline expression in flies differs substantially from somatic expression, requiring particular basal promoters and often specialised 3'UTRs (Ni et al., 2011; Rørth, 1998). Therefore, we used ovaries to test the fTRG library and probed the expression of 115 randomly selected lines in germline cells versus somatic cells during oogenesis (**Figure 3A**). From the 115 lines 91 (79 %) showed detectable expression during oogenesis, with 45 lines being expressed in both, germ cells and the somatic epithelial cells

(**Figure 3B, C** and **Supplementary File 3**). 76 (66 %) fTRG lines showed interesting expression patterns restricted to subsets of cells or to a subcellular compartment (**Figure 3B - D**). For example, Tan-GFP is expressed in germline stem cells only, whereas the ECM protein Pericardin (Prc-GFP) is concentrated around the neighbouring cap cells and the transcription factor Delilah (Dei-GFP) is specifically localised to the nuclei of somatic stem cells, which will give rise to the epithelial cells surrounding each egg chamber (**Figure 3A, C**). In early egg chambers Reph-GFP is expressed in germ cells only, whereas the ECM protein Viking (Vkg-GFP) specifically surrounds all the somatic epithelial cells. Interestingly, the transcription factor Auracan (Ara-GFP) is only expressed in posterior follicle cells, whereas the putative retinal transporter CG5958 is only detectable in the squamous epithelial cells surrounding the nurse cells (**Figure 3C**).

We further investigated the subcellular localisation of the tagged proteins, which revealed a localisation for the RNA helicase l(2)35Df to all nuclei, whereas the predicted C_2H_2-Zn-finger transcription factor Crooked legs (Crol-GFP) is restricted to the nuclei of the epithelial cells (**Figure 3D**). Interestingly, Corolla-GFP is exclusively localised to the oocyte nucleus in early egg chambers. This is consistent with the function of Corolla at the synaptonemal complex attaching homologous chromosomes during early meiosis (Collins et al., 2014). In contrast, the uncharacterised homeobox transcription factor E5 (E5-GFP) is largely restricted to the nuclei of anterior and posterior epithelial cells (**Figure 3D**). Apart from nuclear patterns, we found a significant number of cortical localisations, including the well characterised Crumbs (Crb-GFP) (Bulgakova and Knust, 2009) and the PDZ-domain containing Big bang (Bbg-GFP) (Bonnay et al., 2013) at the apical cortex of the epithelial cells, the Na^+/K^+ transporter subunit Nervana 2 (Nrv2-GFP) at the lateral epithelial membrane, and the EGF-signalling regulator Star (S-GFP) as well as the TGF-β receptor Saxophone (Sax-GFP) localised to the cortex or membrane of the germ cells **(Figure 3D**

285 and **Supplementary File 3**). Furthermore, we find a perinuclear enrichment for the
286 uncharacterised predicted NAD binding protein CG8768, and oocyte enrichments for the
287 Tom22 homolog Maggie (Mge-GFP) (Vaskova et al., 2000), the glycosyltransferase
288 Wollknäuel (Wol-GFP) (Haecker et al., 2008) and the TGF-α homolog Gurken (Grk-GFP),
289 the latter with its well established concentration around the oocyte nucleus (Neuman-
290 Silberberg and Schüpbach, 1993), where it colocalises with endogenous Grk protein
291 (**Figure 3D** and **Figure 3-figure supplement 1A, B**).

292 We did not perform genetic rescue assays for all of lines examined for protein
293 localisation. However, even tagged proteins, for which the rescue assay failed, such as
294 Vkg-GFP, can result in an informative expression pattern (**Figure 3D, Table 2**).
295 Obviously, an independent validation of expression patterns established solely based on a
296 tagged transgenic reporters is advisable.

297 To test if genes expressed from the FlyFos system also undergo normal post-
298 transcriptional regulation we analysed the *osk-GFP* line, which was recently used as a label
299 for germ granules (Trcek et al., 2015). *osk* mRNA is transcribed from early stages of
300 oogenesis onwards in the nurse cell nuclei and specifically transported to the oocyte, where
301 it localises to the posterior pole (Ephrussi et al., 1991; Kim-Ha et al., 1991). Only after the
302 mRNA is localised, it is translated from stage 9 onwards (Kim-Ha et al., 1995). Indeed,
303 fosmid derived *osk-GFP* mRNA localises normally during all stages of oogenesis and its
304 translation is repressed during mRNA transport, as Osk-GFP protein can only be detected
305 at the posterior pole from stage 9 onwards (**Figure 3-figure supplement 2A, B**). *osk*-GFP
306 also rescues all aspects of an *osk* null allele (**Figure 2B, C**) and Osk-GFP colocalises with
307 endogenous Osk protein (**Figure 3-figure supplement 1C, D**). Additionally, we
308 discovered a post-transcriptional regulation for *corolla*. *corolla-GFP* mRNA localises to
309 the oocyte at stage 6 and Corolla-GFP protein is transported into the oocyte nucleus.

However, despite the presence of the *corolla-GFP* mRNA at stage 8, Corolla protein is undetectable, suggesting either a translational block of the RNA or targeted degradation of the protein (**Figure 3-figure supplement 2C - F**). Taken together, these expression and protein localisation data recapitulate known patterns accurately and identify various unknown protein localisations in various cell types during oogenesis, and thus emphasise the value of the fly TransgeneOme resource.

Live in toto **imaging of fTRG lines during embryogenesis**

For many genes, the expression patterns at the mRNA level are particularly well characterised during *Drosophila* embryogenesis (Hammonds et al., 2013; Tomancak et al., 2002; 2007). However, *in situ* hybridisation techniques on fixed tissues do not visualise dynamics of expression over time and thus do not allow tracking of the expressing cells during development. As our tagging approach enables live imaging at endogenous expression levels we set out to test if *in toto* imaging using the SPIM (Selective Plane Illumination Microscopy) technology (Huisken et al., 2004) can be applied to the fly TransgeneOme lines. We pre-screened a small subset of lines (**Table 3**) and selected the Na^+/K^+ transporter subunit Nrv2, as it shows high expression levels, for long-term time-lapse live imaging with a multi-view dual-side SPIM (Huisken and Stainier, 2007). During embryogenesis Nrv2 expression was reported in neurons (Sun et al., 1999) and glial cells (Younossi-Hartenstein et al., 2002). Interestingly, we find that Nrv2-GFP is already expressed from stage 11 onwards in most likely all cell types, where it localises to the plasma membrane (**Figure 4A - C**), similarly to its localisation in ovaries (**Figure 3D**). The expression level increases during stage 15 in all cells, with a particularly strong increase in the developing central nervous system (CNS) labelling the CNS and motor neuron

membranes (**Figure 4, Video 1**[1]). These live *in toto* expression data are consistent with expression data of a recently isolated GFP trap in *nrv2* (Lowe et al., 2014), thus validating our methodology.

We wanted to extend our approach beyond highly expressed structural genes towards transcription factors that enable to follow cell lineages in the embryo. For this purpose we crossed the fTRG line of the homeobox transcription factor *gooseberry* (Gsb-GFP) to H2A-mRFPruby, which labels all nuclei, and recorded a two-colour multi-view dual-side SPIM Video. We find that Gsb-GFP is expressed in the presumptive neuroectoderm of the head region, labelling segmentally reiterated stripe-like domains at stage 10 (**Figure 4-figure supplement 1A, B, Video 2**) as was described from fixed images (Gutjahr et al., 1993). Focusing on the deuterocerebral domain, we could reconstruct the delamination of two neuroblasts, which up-regulate Gsb-GFP while initiating their asymmetric divisions (**Figure 4-figure supplement 1C - F**). It was possible to individually follow their neural progeny. Gsb-GFP expression also allowed us to directly follow the gradual down-regulation of Gsb-GFP in ectodermal cells that remained at the head surface after neuroblast delamination. As opposed to the neuroblasts, these cells, which give rise to epidermis, did not divide at all, or underwent only one further division (**Figure 4-figure supplement 1G - J, Video 2**).

gsb is in part required for *gooseberry-neuro* (*gsb-n*; also called *gsb-d*) expression (He and Noll, 2013). Notably, expression of Gsb-n-GFP (fTRG line 513) becomes detectable only at the end of germ-band extension (end of stage 11) in the developing CNS, where it lasts until stage 17 (**Figure 4-figure supplement 2**, **Video 3**). Again this is consistent with published immuno-histochemistry data (Gutjahr et al., 1993; He and Noll, 2013). We conclude that our fly TransgeneOme library can be used for live *in toto* imaging,

[1] Examine raw data in BigDataViewer (Fiji -> Plugins -> BigDataViewer -> Browse BigDataServer and http://bds.mpi-cbg.de:8087

even for transcription factors expressed at endogenous levels. This will be of significant importance for on-going efforts linking the transcription factor expression patterns of embryonic neuroblasts to the morphologically defined lineages that structure the larval and adult *Drosophila* brain (Hartenstein et al., 2015; Lovick et al., 2013; Pereanu, 2006).

Expression of fTRG lines in the adult thorax

Cells and tissues in the embryo are not yet terminally differentiated. To apply our TransgeneOme library to fully differentiated tissues we decided to study tissues of the adult thorax. We scored expression in the large indirect flight muscles (IFMs), in leg muscles, in the visceral muscles surrounding the gut, in the gut epithelium, the tendon epithelium, the trachea and the ventral nerve cord including the motor neurons. In total, we found detectable expression in at least one tissue for 101 of 121 (83.5 %) analysed fTRG lines, thus creating a large number of valuable markers for cell types and subcellular structures (**Table 4, Supplementary File 4**).

The large IFMs are fibrillar muscles, which have a distinct transcriptional program resulting in their distinct morphology (Schönbauer et al., 2011). This is recapitulated by the expression of Act88F-GFP, which localises to the thin filaments of IFMs only (**Figure 5A - C**), whereas Mlp84B-GFP is not expressed in IFMs but at the peripheral Z-discs of leg and visceral muscles only (**Figure 5D - F**), similar to the published localisation in larval muscle (Clark et al., 2007). We find various dotty patterns indicating localisation to intracellular vesicles; a particularly prominent example is Tango1-GFP in the midgut epithelium (**Figure 5G, H, Supplementary File 4**). Tango1 regulates protein secretion in S2 cells, where it localises to the Golgi apparatus upon over-expression (Bard et al., 2006), suggesting that the pattern described here is correct. We find Par6 with an in analogy to other epithelia expected apical localisation (Hutterer et al., 2004) in the epithelium of the

proventriculus and in trachea (**Figure 5I, J**), whereas we identified a surprising pattern for the TRP channel Painless (Tracey et al., 2003). Pain-GFP is not only highly expressed in motor neurons (**Figure 5K**) but also in a particular set of small cells within the gut epithelium and most surprisingly, in the tendon cells to which the IFMs attach (**Figure 5L, M**). To clarify the identity of the Pain-GFP positive cell type in the gut, we co-stained with the differentiated enteroendocrine cell marker Prospero (Ohlstein and Spradling, 2005), however did not find any overlap with the Pain-GFP positive cells (**Figure 5Q**). This suggests that the small, likely diploid, Pain-GFP positive cells are either enteroblasts or intestinal stem cells (ISCs), the source of all enterocytes and enteroendocrine cells that build the gut epithelium (Jiang and Edgar, 2011). At this point, we can only speculate that Pain might be involved in mechanical stretch-sensing in these cell types. We have also tagged various ECM components, with LamininB1 (LanB1-GFP), LamininA (LanA-GFP) and BM40-SPARC resulting in the most prominent expression patterns. All three ensheath most adult tissues, particularly the muscles (**Figure 5N, O**, **Figure 5-figure supplement 1A, B, E, F**). Interestingly, LanA-GFP and LanB1-GFP also surround the fine tracheal branches that penetrate into the IFMs, whereas BM40-SPARC is only detected around the large tracheal stalk and the motor neurons (**Figure 5P**, **Figure 5-figure supplement 1C, D, G, H**). Finally, we also detected prominent neuromuscular junction (NMJ) markers; the IκB homolog Cactus shows a distinct pattern on leg muscles, visceral muscles and IFMs, the latter we could confirm by co-staining with the neuronal marker Futsch (**Figure 5-figure supplement 1I - M**). Interestingly, such a NMJ pattern for Cactus and its binding partner Dorsal has been shown in larval body muscle by antibody stainings (Bolatto et al., 2003). Together, these results suggest that our fly TransgeneOme library provides a rich resource for tissue-specific markers in the adult fly that can routinely be used to visualise subcellular compartments in various tissues.

To further validate the advantages of our TransgeneOme lines to label subcellular structures we imaged the large IFMs of the same 121 lines at high resolution. We found various markers for the thick filaments (e.g. the myosin associated protein Flightin, Fln-GFP) (Vigoreaux et al., 1993), for the myofibrils (e.g. the protein kinase Fray-GFP), the M-lines (e.g. the titin related protein Unc-89/Obscurin-GFP) (Katzemich et al., 2012), the Z-discs (e.g. CG31772-GFP) and the muscle attachment sites (e.g. Integrin-linked-kinase, Ilk-GFP). Furthermore, we identified markers for the T-tubules (e.g. Dlg1-GFP), for different vesicular compartments (e.g. the TGFβ receptor Baboon-GFP) and for mitochondria (CG12118) within the IFMs (**Figure 6, Table 4, Supplementary File 4**). The latter was confirmed by co-labelling the mitochondria with an antibody against the mitochondrial ATPase (complex V α subunit) (Cox and Spradling, 2009) (**Figure 6-figure supplement 1**). Additionally, we documented the nuclear localisation in IFMs and leg muscles for a variety of fTRG proteins, including the uncharacterised homeodomain protein CG11617 and the C_2H_2 Zinc-fingers CG12391 and CG17912 (**Figure 6-figure supplement 2A - C, E - G**); both of the latter result in flightless animals when knocked-down by muscle-specific RNAi (Schnorrer et al., 2010) suggesting that these genes play an essential role for IFM morphogenesis or function. Interestingly, the well characterised C_2H_2 Zinc-finger protein Hunchback (Hb) is only localised to leg muscle nuclei, but absent from IFMs suggesting a leg muscle-specific function of Hb (**Figure 6-figure supplement 2G, H**).

However, differences between muscle types are not only controlled transcriptionally but also by alternative splicing (Oas et al., 2014; Spletter and Schnorrer, 2014; Spletter et al., 2015). To investigate if our tagging approach can be used to generate isoform-specific lines, we have chosen two prominent muscle genes, *mhc* and *rhea* (the fly Talin), both of which have predicted isoforms with different C-termini (**Figure 6-figure supplement 3A, H**). Interestingly, we found that Mhc-isoforms K, L, M are expressed in IFMs and all leg

muscles, however the predicted Mhc-isoforms A, F, G, B, S, V with the distal STOP codon are selectively expressed in visceral muscle and in a subset of leg muscles, however absent in adult IFMs (**Figure 6-figure supplement 3B - G**). Even more surprisingly, while the long 'conventional' *rhea* (Talin) isoforms B, E, F, G show the expected localisation to muscle attachment sites in IFMs and leg muscles (Weitkunat et al., 2014), the short Talin-isoforms C and D do not localise to muscle attachment sites, but are selectively concentrated at costamers of leg muscles (**Figure 6-figure supplement 3I - N**). Hence, the tagged proteins of our TransgeneOme library are ideally suited to label subcellular compartments and protein complexes, and in some cases they can even distinguish between closely related protein isoforms.

GFP-tagged proteins largely recapitulate the endogenous protein localisation

Tagging of any protein can in principle affect its localisation pattern in a cell. To investigate the reliability of the observed GFP-tagged protein patterns, we selected eight different fTRG lines with specific GFP patterns in adults described above (LanA, LanB (not shown), Par6, Mlp84B, Mhc, Fln, Unc89/Obscurin and Dlg1), for which reliable antibodies against the corresponding proteins were readily available. In all cases we observed a high degree of overlap between the pattern revealed by staining with anti-GFP antibody and the respective specific antibody staining pattern in the same transgenic line. This suggests that the tagged proteins expressed in the fTRG lines and the endogenous proteins co-localised to a large extent (**Figure 7A - D, I - L**). To rule out that the tagged protein somehow induces the endogenous protein to adopt an abnormal pattern, we compared the localisation patterns in the fTRG lines (with the protein specific antibody that visualizes both the tagged and untagged endogenous form of the protein) to a wild type strain, which only expresses the endogenous protein (**Figure 7E - H, M - P**). Only in one

458 fTRG line, expressing the highly expressed short Mhc isoforms K, L, M-GFP tagged, we
459 found an abnormally broad anti-Mhc pattern in IFMs, however not in leg muscles
460 compared to wild type (**Figure 7D, H, L, P**). This pattern is explained by an abnormal
461 myofibril morphology in the IFMs of the fTRG500 line, possibly because of an increased
462 Mhc to actin ratio (4 copies vs. 2 copies), for which IFMs are particularly sensitive (Cripps
463 et al., 1994).

464 Tagging a protein may modify its turn-over rates and thus its expression levels,
465 despite preserving its localisation. To investigate if our tagging approach generally changes
466 protein levels we chose three different tagged proteins, expressed in different tissues, for
467 which we had functional antibodies and the expected 40 kDa shift caused by the tag should
468 result in a detectable shift compared to the size of the untagged endogenous protein. We
469 made total protein extracts from adults males and run Western blots. When probing with an
470 antibody against the tag we find the expected sizes for the IFM-specific Fln-GFP, the leg
471 muscle-specific Mlp84B-GFP and the broader expressed Dlg1-GFP, the latter running in
472 several bands due to splice isoforms (**Figure 7Q**). Probing the same extracts with specific
473 antibodies against the respective proteins shows that both Fln-GFP and Dlg1-GFP levels
474 are comparable to the endogenous protein, whereas Mlp84B-GFP is expressed at a lower
475 level (**Figure 7Q**). The latter may be caused by the reduced affinity to the thick filament
476 due to the tag resulting in an unstable protein. Together, these data demonstrate that many
477 of the tagged proteins colocalise with the respective endogenous proteins, as has been
478 observed in other large-scale tagging approaches (Stadler et al., 2013), however exact
479 expression levels can be different from the wild-type level in some cases. Thus, the fTRG
480 library is a valuable collection of strains to study *in vivo* protein localisation.

481

482 **Expression of the fTRG lines in the living pupal thorax**

An attractive application of the fly TransgeneOme library is live *in vivo* imaging. In the past, we had established live imaging of developing flight muscles in the pupal thorax using over-expressed marker proteins (Weitkunat et al., 2014). Here, we wanted to test, if live imaging of proteins at endogenous expression levels is also possible within the thick pupal thorax. We selected six fTRG lines for well established genes and indeed could detect expression and subcellular localisation for all of them using a spinning-disc confocal microscope either at the level of the pupal epidermis or below the epidermis, in the developing flight muscles, or both (**Figure 8**). The adducin-like Hts-GFP labels the cytoplasm of fusing myoblasts from 10 to 20 h APF (after puparium formation) and the developing SOPs (sensory organ precursors) with a particular prominent concentration in developing neurons and their axons (**Figure 8B - E**). In contrast, Dlg1-GFP localises to cell-cell-junctions of the pupal epidermis and to a network of internal membranes in the developing IFMs (**Figure 8F - I**) that may resemble developing T-Tubules, for which Dlg1 is a well established marker (Razzaq et al., 2001). Interestingly, the long isoforms of Talin-GFP (*rhea* isoforms B, E, F, G) are largely in the cytoplasm and at the cortex of the epidermal cells, with a marked enrichment in the developing SOPs at 10 to 20 h APF (**Figure 8J, K**). Further, Talin-GFP is strongly concentrated at muscle attachment sites of developing IFMs from 24 h onwards (**Figure 8L, M**) consistent with antibody stainings of IFMs (Weitkunat et al., 2014).

The dynamics of the extracellular matrix is little described thus far as very few live markers existed. Hence, we tested our LamininB1 fosmid and found that LanB1-GFP is readily detectable within the developing basement-membrane basal to the epidermal cells of the pupal thorax at 10 h APF (**Figure 8N**). It also labels the assembling basement-membrane around the developing IFMs from 16 to 30 h APF without a particularly obvious concentration at the muscle attachment sites (**Figure 8O - Q**). To specifically visualise the

developing IFMs we chose Actin88F, which is specifically expressed in IFMs and a few leg muscles (Nongthomba et al., 2001). We find that the Act88F-GFP fTRG line indeed very strongly labels the IFMs from about 18 h APF but is also expressed in the developing pupal epidermis again with an enrichment in the forming SOPs from 10 to 20 h APF (**Figure 8R - U**). The latter is not surprising as Act88F-lacZ reporter has been shown to also label the developing wing epithelium (Nongthomba et al., 2001), again suggesting that our fTRG line recapitulates the endogenous expression pattern. Finally, we tested the βTub60D fTRG-line, as βTub60D was reported to label the myoblasts and developing myotubes in embryonic and adult muscles (Fernandes et al., 2005; Leiss et al., 1988; Schnorrer et al., 2007). Indeed, we detect βTub60D-GFP in fusing myoblasts and the developing IFMs, with particularly prominent label of the microtubule bundles at 24h APF (**Figure 8V - Y**). In addition, βTub60D-GFP also strongly marks the developing hairs of the sensory organs of the pupal epidermis (**Figure 8X**, see also **Video 6**).

In order to test, if the fly TransgeneOme lines and the sGFP-tag are indeed suited for long-term live imaging in pupae we chose Act88F-GFP and βTub60D-GFP and imaged the developing IFMs for more than 19 h with a two-photon microscope using an established protocol for over-expressed markers (Weitkunat and Schnorrer, 2014). For both proteins we can detect strongly increasing expression after 18 h APF in the developing IFMs, with Act88F-GFP being restricted to the myotubes and the developing myofibrillar bundles (**Video 4**, **Figure 8-figure supplement 1A - F**) whereas βTub60D-GFP also labels the fusing myoblasts and is largely incorporated into prominent microtubule bundles (**Video 6**, **Figure 8-figure supplement 1L - Q**).

As photo bleaching was no serious problem in these long Videos we also recorded Videos at higher time and spatial resolution. We labelled the developing IFMs with Act88F-GFP and the myoblasts with a *him*-GAL4, UAS-palm-Cherry and acquired a 3D

stack every two minutes using a spinning disc-confocal. This enabled us to visualise single myoblast fusion events in developing IFMs of an intact pupa (**Video 5**, **Figure 8-figure supplement 1G - K**). The six dorsal longitudinally oriented IFMs develop from three larval template muscles to which myoblasts fuse to induce their splitting into six myotubes (Fernandes et al., 1991). Using high resolution imaging of the βTub60D-GFP line we find that most myoblasts fuse in the middle of the developing myotube during myotube splitting, with prominent microtubules bundles located at the peripheral cortex of the splitting myotube (**Video 7, Figure 8-figure supplement 1R**). These prominent microtubules bundles are then relocated throughout the entire developing myotube (**Video 7**, **Figure 8-figure supplement 1S - V**). Taken together, these live imaging data suggest that many fTRG lines will be well suited for high resolution live imaging of dynamic subcellular protein localisation patterns in developing *Drosophila* organs. This will strongly expand the set of live markers available for research in flies.

Fly TransgeneOme library as bait for proteomics

For the proper composition, localisation and *in vivo* function of most protein complexes endogenous expression levels of the individual components are critical (Rørth et al., 1998; Tseng and Hariharan, 2002). Hence, the TransgeneOme library would be an ideal experimental set-up to purify protein complexes from different developmental stages using endogenous expression levels of the bait protein. In principle, all the small affinity tags (TY1, V5, FLAG) (**Figure 1-figure supplement 1**) can be used for complex purifications. The presence of precision and TEV cleavage sites even allow two-step purifications. For proof of principle experiments, we selected four tagged proteins as baits: Ilk, Dlg1, Talin and LanB1, and analysed two different developmental stages. In each case we homogenised hundred 24 to 48 h pupae and hundred adult flies per experiment and mixed the cleared

lysate with a GFP antibody matrix to perform single step affinity enrichment and mass-spec analysis modified from the QUBIC protocol (Hein et al., 2015; Hubner et al., 2010; Keilhauer et al., 2014). Each affinity-enrichment was performed in triplicate and intensity profiles of all identified proteins were quantified in a label-free format by running all 30 purifications consecutively on the same Orbitrap mass-spectrometer and analysing the data with the MaxQuant software suite (Cox and Mann, 2008; Cox et al., 2014) (**Supplementary File 5**). Interestingly, enriching Ilk-GFP from both, developing pupae and adult flies, recovered the entire Ilk, PINCH, Parvin, RSU-1 complex (**Figure 9**), which had previously been purified *in vitro* from *Drosophila* S2 cells (Kadrmas et al., 2004) and mammalian cells (Dougherty et al., 2005; Tu et al., 2001) giving us confidence in our methodology. We also successfully enriched Talin-GFP from pupae or adults, however did not identify an obvious strong and specific binding partner (**Figure 9**, **Supplementary File 5**). In contrast, we identified Mesh as a novel interactor of Dlg1 from pupae and adult flies. Mesh colocalises with Dlg1 at septate junctions of the embryonic *Drosophila* midgut, however a molecular interaction of both proteins was not established (Izumi et al., 2012). Finally, we purified the laminin complex by pulling on LanB1, which recovered LanB2 and LanA roughly stoichiometrically, both from pupae and adult flies, as had been found in cell culture experiments (Fessler et al., 1987), showing that extracellular matrix complexes can also be purified from *in vivo* samples with our methodology. In summary, these data demonstrate that interaction proteomics with the fly TransgeneOme library can confirm known interaction partners and discover novel *in vivo* complex members, making the system attractive for a variety of biochemical applications.

Discussion

The TransgeneOme resource presented here adds a new powerful component to the arsenal of tools available to the *Drosophila* research community. It complements the genetic resources for gene disruption and localisation (Buszczak et al., 2007; Lowe et al., 2014; Morin et al., 2001; Nagarkar-Jaiswal et al., 2015; Quiñones-Coello et al., 2007; St Johnston, 2012; Venken and Bellen, 2012; Venken et al., 2011) with a comprehensive genome-scale library that does not suffer the biases of random mutagenesis. Analogously to the powerful MiMIC system (Nagarkar-Jaiswal et al., 2015; Venken et al., 2011) the TransgeneOme resource is versatile and can be adapted to the developments in tag chemistry and to various specialised applications. Although the resource is designed to study behaviour of proteins, it can for example be converted into a toolkit for live imaging of mRNAs. By designing a tagging cassette with an array of MS2 binding sites (Forrest and Gavis, 2003) the existing 'pre-tagged' TransgeneOme can be converted into an MS2-tagged TransgeneOme by a single liquid culture recombineering step in bacteria.

However, any new TransgeneOme has to be transformed into flies and this process still represents a significant bottleneck. We present here an optimised protocol for transgenesis of fosmid size clones into *Drosophila melanogaster* that was adapted from a previous large-scale transgenesis project (Venken et al., 2010). It took three years and four dedicated technicians to generate the 880 fly lines presented in this study. Although, the systematic transgenesis is a continuing process in our laboratories, the value of the TransgeneOme collection is highlighted by the fact that any specific set of genomically tagged gene clones is now available. These can be efficiently transformed by in house transgenesis of *Drosophila* labs around the world using the optimised protocol presented here.

One caveat of designed expression reporters is the necessity to place the tag into a defined position within the gene model. We chose to generate our 'pre-tagged' collection at the most commonly used C-terminus predicted by the gene model, thus labelling most isoforms. In some cases a tag at the C-terminus will inactivate the protein, however such a reagent can still be useful for visualising the protein, although the result needs to be treated with care. This has been demonstrated for a number of sarcomeric protein GFP-traps, some of which lead to lethality when homozygous, yet result in interesting localisation patterns when heterozygous (Buszczak et al., 2007; Morin et al., 2001). Similarly, we found an interesting localisation pattern for BM40-SPARC-GFP despite being non functional. In some cases the tag may result in a mis-localisation of the tagged protein, compared with the untagged endogenous one, in particular when the tag interferes with protein function. For particular genes, it will be useful to tag differential protein isoforms, which in some cases can be done by tagging alternative C-termini, as shown here for *Mhc* and *rhea*. However, tagging a particular isoform requires a very informed construct design, which cannot easily be automated at the genome scale.

A functional GFP-tagged gene copy, as present in our fTRG lines, can also serve as a ‘conditional’ allele, when crossed into the mutant background and combined with deGradeFP (degrade Green Fluorescent Protein), an elegant method expressing a nanobody against GFP, coupled to a degradation signal in a tissue- and stage-specific manner (Caussinus et al., 2011; Neumuller et al., 2012). As the expression of the nanobody can be turned on or off, it is also possible to reversibly remove the tagged protein, as recently shown for the GFP-tagged MiMIC lines (Nagarkar-Jaiswal et al., 2015). This introduces yet an other level of experimental manipulation, directly controlling protein levels at a given developmental stage.

628 Genome engineering is experiencing a tremendous growth with the introduction of
629 CRISPR/Cas technology and it will be only a matter of time before a larger collection of
630 precisely engineered fusion proteins at endogenous loci will become available in flies.
631 However to date, such examples are still limited to a few genes (Baena-Lopez et al., 2013;
632 Gratz et al., 2014; Port et al., 2014; Zhang et al., 2014), which had been carefully picked
633 and were individually manipulated with custom-designed, gene-specific tools. It remains to
634 be tested which proportion of such engineered loci will be fully functional and thus
635 potentially superior to the fTRG collection. However, having a transgenic third allele copy,
636 as is the case in our TransgeneOme collection, might even be advantageous, if the tagging
637 interferes with protein function, because the TransgeneOme lines still retain two wild-type
638 endogenous gene copies. In some cases, addition of GFP might destabilise the protein,
639 regardless of N- or C-terminal fusion, as recently shown for the Engrailed protein
640 (Sokolovski et al., 2015). However, our ability to detect the protein product in the vast
641 majority of our tagged lines argues that this could be a relatively rare, gene specific
642 phenomenon. Nevertheless, caution should be taken with respect to protein turnover
643 dynamics of any tagged protein.

644 An additional advantage of our transgenic resource, independent of whether or not
645 the gene is tagged, is that it can be used to rescue a classic genetic mutation and thus
646 formally demonstrate that any observed phenotype is caused by the mutation in the studied
647 gene. This cannot easily be done when modifying the endogenous gene copy by a MiMIC
648 insertion or a CRISPR induced mutation. Thus our resource complements previously
649 published collections of genomic constructs (Ejsmont et al., 2009; Venken et al., 2009).

650 Together, the FlyFos library, the fly TransgeneOme library and the fTRG collection
651 of strains, enable genome-scale examination of expression and localisation of proteins
652 comparable with the high-throughput mRNA *in situ* screens (Tomancak et al., 2002; 2007).

Our data for tagged Oscar protein show that fosmid-based reporters can in principle recapitulate all aspects of gene expression regulation at transcriptional and post-transcriptional levels. It will be particularly interesting to combine the spatial expression data of mRNAs with that of proteins. Since many transcripts show subcellular localisation patterns in various developmental contexts (Jambor et al., 2015; Lécuyer et al., 2007), the question arises whether RNA localisation generally precedes localised protein activity. Systematic examination of protein patterns expressed from localised transcripts in systems such as the ovary will provide a genome-scale overview of the extent and functional role of translational control. At the tissue level, the patterns of mRNA expression may be different from the patterns of protein expression, for example due to translational repression in some cells or tissue specific regulation of protein stability, as shown here for the Corolla protein. The combined mRNA and protein expression patterns may therefore uncover a hidden complexity in overall gene activity regulation and the fTRG lines will help to reveal these combinatorial patterns in a systematic manner.

The fTRG lines faithfully recapitulate gene expression patterns in ovaries, embryos, larvae, pupae and adults suggesting that they can be used to visualise proteins in every tissue during the life cycle of the fly. This includes adult tissues such as the flight or leg muscles, which thus far had not been subjected to systematic protein expression and localisation studies. However, due to their size and the conservation of the contractile apparatus these tissues are particularly attractive to study with this new resource. In general, antibody or FISH (Fluorescent In Situ Hybridisation) stainings with a single standard anti-tag reagent are easier to optimise, compared to antibody stainings or mRNA *in situ* hybridisations with gene specific antibodies/probes. This simplicity makes it possible to explore the expression of the available genes across multiple tissues, as has been done for the *rab* collection (Dunst et al., 2015). Such an approach is orthogonal to the

678 collections of expression data generated thus far, in which many genes were examined
679 systematically but only at particular stages or in certain tissues, i.e. embryos or ovaries
680 (Jambor et al., 2015; Lécuyer et al., 2007; Tomancak et al., 2007). We are confident that
681 the analysis of regularly studied as well as less explored *Drosophila* tissues will be
682 stimulated by the fTRG collection.

683 When protein expression levels are sufficiently high, the fusion proteins can be
684 visualised by live imaging approaches in intact animals. It is difficult to estimate the
685 absolute expression levels required for live visualisation, as this depends on the imaging
686 conditions, the accessibility and transparency of the tissue and importantly on the observed
687 protein pattern. A strongly localised protein can result in a very bright local signal, such as
688 Talin or Ilk at the muscle attachment sites or Gsb in the neuroblast nuclei, compared to a
689 protein homogenously distributed throughout the entire cell. Given optimal imaging
690 conditions, we estimate conservatively that about 50 % of the tagged proteins can be
691 visualised live, if they are expressed in tissues accessible to live imaging. In particular for
692 tissues, such as the adult legs, antennae or the adult fat body, which are difficult to dissect
693 and stain without losing tissue integrity, these live markers should be enormously
694 beneficial.

695 One important limitation for examining the pattern of protein expression is the
696 accessibility of the tissue of interest for imaging. We have shown that light sheet
697 microscopy can be used to image the dynamics of tagged protein expression throughout
698 embryogenesis. We further demonstrated that two-photon microscopy can be applied to
699 study protein dynamics during muscle morphogenesis in developing pupae. Other confocal
700 or light sheet based imaging paradigms could be adapted for *in toto* imaging of living or
701 fixed and cleared specimen from other life cycle stages. Establishing standardized protocols

for preparation, staining and imaging of *Drosophila* stages, isolated tissues and organs will be necessary to realise the full potential of the fTRG collection.

Protein interaction data in fly are available from a number of studies (Formstecher et al., 2005; Giot et al., 2003; Guruharsha et al., 2011). These results were generated using yeast two-hybrid, or over-expression in a tissue culture system, followed by affinity purification and mass spectrometric analysis. Despite high-throughput, these approaches face the problem that the interacting proteins might not be present at the same place within a cell, or not even co-expressed in a developing organism. This is circumvented by affinity purifications of endogenously expressed proteins, which thus far at genome-scale was only reported from yeast (Gavin et al., 2002; Ho et al., 2002; Krogan et al., 2006). In higher organisms, BAC-based systems, which are closely related to our fosmid approach, elegantly solved these issues, as shown by a recent human interactome study (Hein et al., 2015).

The collection of transgenic fTRG lines covers currently only about 10 % of the available tagged TransgeneOme clones. Expanding the fly collection to include most genes of the genome and importantly characterising the expression of the tagged proteins by imaging in various biological contexts is best achieved by spreading the clones and transgenic lines amongst the community of researchers using *Drosophila* as a model system. Therefore, all transgenic lines are available from the VDRC stock collection and all TransgeneOme clones from Source Biosciences. Despite the expanding CRISPR-based genome engineering technologies, the fTRG collection will continue to be an important resource for the fly community, in particular, if the full functionality of certain fTRG lines has been demonstrated, as we did here for a selection of important developmental regulators. As with many genome-scale resources it is typically easier to produce them than to fully characterise and exploit their potential. Comprehensive generation of thousands of

727 transgenes and their thorough analysis takes time; it took us 4 years to assemble the
728 collection presented here. Development of protocols and techniques to image these
729 collections of tagged lines and assembling open access databases to share the data needs to
730 continue and will eventually become useful also for the characterisation of resources whose
731 production began only recently.

732 Wangler, Yamamoto and Bellen convincingly argued that the *Drosophila* system
733 remains an indispensable model for translational research because many essential fly genes
734 are homologs of Mendelian disease genes in humans (Wangler et al., 2015). Yet, even after
735 decades of research on fruit flies only about 2,000 of the estimated 5,000 lethal mutations
736 have been investigated. Resources like ours will therefore provide essential functional
737 information about gene expression and localisation in *Drosophila* tissues that can serve as a
738 starting point for the mechanistic understanding of human pathologies and their eventual
739 cures.

Materials and Methods

TransgeneOme clone engineering

Fosmids were engineered as described previously (Ejsmont et al., 2009; 2011), except for the inclusion of the 'pre-tagging' step in the genome-wide TransgeneOme set. All tagging cassettes were generated from synthetic DNA and cloned into R6K carrying plasmids, which require the presence of the *pir* gene product for replication (Metcalf et al., 1996). The *pir* gene is not present in the FlyFos library host strain, thereby ensuring near-complete lack of background resistance in the absence of the correct homologous recombination event.

Details of the recombineering steps are as follows (**Figure 1B**): Step 1. The *E. coli* cells containing a FlyFos clone covering the gene locus of interest are transformed with the pRedFlp plasmid, containing the genes necessary for the homologous recombination and the Flp recombinase under independently inducible promoters. Step 2. Next, a 'pre-tagging' cassette carrying an antibiotic resistance gene (NatR, nourseothricin resistance) surrounded by regions of homology to all specific tagging cassettes (**Figure 1-figure supplement 1**) and flanked by gene specific homology arms is electroporated as linear DNA fragment produced by PCR. By combination of induced (L-rhamnose) pRedFlp homologous recombination enzyme action and strong selection with a cocktail of three antibiotics (one to maintain the fosmid (chloramphenicol, Cm), one to maintain the pRedFlp (hygromycin, Hgr) and nourseothricin (Ntc) to select for the inserted fragment) the electroporated linear 'pre-tagging' fragment becomes inserted in front of the STOP codon of the gene of interest. Step 3. The 'pre-tagging' cassette is exchanged for a cassette of the chosen tag coding sequence including an FRT-flanked selection / counter selection marker (rpsL-neo). This cassette is now universally targeting the homologous sequences shared by the tagging and pre-tagging cassettes and is produced in bulk by restriction

765 enzyme mediated excision from a plasmid. Note that in this way, no PCR-induced
766 mutations can be introduced at this step. Step 4. Upon Flp induction (with
767 anhydrotetracycline), the rpsL-neo cassette is excised, leaving a single FRT site, positioned
768 in frame after the tag coding sequence. In this way, the endogenous STOP codon and the
769 3'-UTR of the tagged gene are used. Step 5. Finally, the recombineering plasmid is
770 removed from the cells containing the engineered fosmids by inhibition of its temperature
771 sensitive origin of replication and release from Hgr selection. The cells are plated on a
772 selective chloramphenicol agar plate, from which a single colony is picked and further
773 validated.
774
775 **NGS-based validation of the TransgeneOme clones**
776 For NGS-based validation of the TransgeneOme library single colonies for each
777 TransgeneOme clone were picked into 96-well plates, grown to saturation and the
778 individual wells of all 96-well plates were pooled into 8 row and 12 column pools. Fosmid
779 DNA was isolated from these pools and barcoded mate pair fragment libraries were
780 prepared using the Nextera matePair library preparation chemistry from Illumina. The
781 library was size selected through agarose gel isolation of approximately 3 kb fragments and
782 sequenced on HiSeq 2500 (Illumina), with paired-end read lengths of 100 bp. Adapters and
783 low quality sequences were trimmed with Trimmomatic0.32. (parameters:
784 ILLUMINACLIP:NexteraPE-PE.fa:2:30:10 LEADING:3 TRAILING:3
785 SLIDINGWINDOW:4:15 MINLEN:36). To detect un-flipped fosmid sequences (where the
786 FLP-mediated excision of selection cassette failed), the read pairs were mapped with
787 Bowtie2 (Langmead and Salzberg, 2012) against the un-flipped tag sequence and the
788 genome. If any read of the mate of the pair mapped to the un-flipped sequence, while the
789 second mate mapped to the genome consistent with the estimated mate pair insert size of

3000 bp ± 1000 bp, the fosmid was flagged as un-flipped and was not further analysed. To identify mutations in the tag and in the immediate genomic surrounding (± 1000 bp), the NGS reads were mapped against the fosmid references that included the flipped tag. The Bowtie2 was set to report only hits where both reads of the pairs map concordantly to the insert size in the tag and in the genome (parameters: -I 2200 -X 3700 --rf --no-discordant --no-unal --no-mixed). PCR duplicated read pairs were removed using samtools1.1 *rmdup* (Li et al., 2009). Mutations were identified by utilising SNP calling implemented in FreeBayes (Garrison and Marth, 1207) using the standard filters and *vcffilter* to eliminate reported SNPs with scores < 20. Finally, in the last step, the information of the row and column pools were compared and summarized using a custom C-program that read the results of the SNP calling and the Bowtie mappings and counted the coverage for each read pair anchored in tag sequence with at least 20 bp. To correct for random PCR or sequencing errors the reported SNPs were compared for the row and column pools of each fosmid and SNPs occurring in both pools with coverage of 3 or more reads were considered as real.

Drosophila stocks and genetic rescue experiments

Fly stocks were maintained using standard culture conditions. All crosses were grown at 25 °C unless otherwise noted. Most of the fly mutant or deficiency strains for the rescue experiments were obtained from the Bloomington *Drosophila* Stock Center and if located on X or 2nd chromosome crossed together with the respective fTRG line. If the mutant gene was located on the 3rd chromosome, it was recombined with the fTRG insertion. Rescue was generally tested in trans-heterozygotes as indicated in **Table 2**. The rescue for 6 genes (*bam, fat, mask, rap, RhoGEF2* and *yki*) was done by others, who communicated or

published the results (**Table 2**). For rescue of flightlessness a standard flight test was used (Schnorrer et al., 2010).

Generation of transgenic fly TransgeneOme (fTRG) lines

Most TransgeneOme fosmid clones were injected into the y[1], w[*], P{nos-phiC31\int.NLS}X; PBac{y+-attP-3B}VK00033 (BL-32542). This stock has white eyes and no fluorescent eye markers, which would interfere with screening for the red fluorescent eye marker used in the FlyFos clones (Ejsmont et al., 2009). A few fosmid clones were also injected into y[1], w[*], P{nos-phiC31\int.NLS}X; PBac{y+-attP-3B}VK00002, with the attP site located on the 2nd chromosome. The *osk-GFP* fosmid was injected into attP40. Please note that all fTRG lines contain the strong 3xP3-dsRed marker (Ejsmont et al., 2009). This is an eyeless derived promoter fragment resulting in dsRed expression in the developing eye and in the brain. This needs to be taken into account when working with the developing or adult brain.

Detailed injection protocol (adapted from (Venken et al., 2010)

A) Bacterial culture of fosmid clones: 1. Inoculate 2 ml LB-medium plus chloramphenicol (Cm 25 µg / ml) with fosmid clone and grow over night at 37 °C. 2. Dilute to 10 ml (9 ml LB-medium + Cm and 1 ml bacterial culture) and add 10 µl 10 % arabinose (final concentration 0.01 %) to induce the fosmid to high copy number. 3. Grow at 37 °C for 5 h and collect the pellet by 10 min centrifugation at 6000 rpm. Pellet can be stored at -20 ºC.

B) Preparation of fosmid DNA: Use the HiPure Plasmid Miniprep Kit from Invitrogen (order number: K2100-03) according to the supplied protocol (MAN0003643) with following modifications: before starting: pre-warm the elution buffer (E4) to 50 °C; step 4: incubate the lysate for 4 min at room temperature; step 5: incubate 4 min on ice before

centrifuging at 4 °C for 10 min; step 8: add 850 µl elution buffer (pre-warmed to 50 °C) to the column; step 9: add 595 µl isopropanol to the elution tube, centrifuge 20 min at 4 °C; wash pellet with 800 µl 70 % ethanol; centrifuge for 2 min; step 12: air dry the pellet for 4 min. Add 20 µl EB-buffer (Qiagen) to the pellet and leave at 4 °C overnight to dissolve without pipetting to avoid shearing of the DNA. Do not freeze the DNA. Adjust the concentration to 250 ng / µl and centrifuge 5 min at full speed before injections. Do not inject DNA older than one week.

C) Embryo injections: Collect young embryos (0 - 30 min) on an agar plate, bleach away the chorion, wash and collect the embryos on a cellulose filter (Whatman 10409814). Align the embryos, transfer them to a glued slide and dry them with silica gel for 10 - 15 min (Roth T199.2). Cover the embryos with Voltalef 10S oil (Lehmann & Voss) and inject the prepared fosmid DNA using a FemtoJet set-up (Eppendorf 5247). The injected DNA should be visible within the embryo. Incubate the injected embryos for 48 h at 18 ºC in a wet chamber and collect the hatched larvae with a brush. Cross the surviving mosaic adults individually to *y, w* males or virgins.

Immuno-stainings and Western blotting

Ovaries: sGFP-protein detection and antibody co-stainings of egg-chambers was done as previously described (Dunst et al., 2015). Detection of the *oskar-GFP* mRNA was performed with a *gfp*-antisense probe (Jambor et al., 2014) and co-staining of *osk* mRNA and Osk protein was done as previously described (Jambor et al., 2011) using a *gfp*-antisense probe and a rabbit anti-GFP antibody (1:1000, ThermoFisher). Rabbit anti-Osk was used 1:3,000 (gift on Anne Ephrussi), mouse anti-Grk was used 1:100 (DSHB).

Adult thoraces: Antibody stainings of adult thoraces, including flight, leg and visceral muscles, were done essentially as described for adult IFMs (Weitkunat and Schnorrer,

2014). Briefly, thoraces from young adult males were fixed for 15 min in relaxing solution (20 mM phosphate buffer, pH 7.0; 5 mM $MgCl_2$; 5 mM EGTA, 5 mM ATP, 4 % PFA) + 0.5 % Triton X-100, cut sagittally with a sharp microtome blade and blocked for 1 hour at room temperature with 3 % normal goat serum in PBS-0.5% Triton X-100. Samples were stained with primary antibodies overnight at 4 ºC, rabbit anti-GFP 1:2000 (Amsbio); mouse anti-Futsch 1:100, mouse anti-Dlg1 clone 4F3 1 :500, mouse anti-Prospero 1:30 (all Hybridoma Bank, DSHB), mouse anti-ATP5a 1:500 (Abcam clone 15H4C4), rabbit anti-Fln (gift of Jim Vigoreaux), rabbit anti-Kc cell Laminin H329 1:2000 (gift of Stefan Baumgartner), rabbit anti-Mlp84B 1:500 (gift of Kathleen Clark), mouse anti-Mhc 1:100 (gift of Judith Saide), Mouse anti-Obscurin 1:500 (gift of Belinda Bullard) rabbit anti-Par6 1:400 (gift of Jürgen Knoblich), washed and incubated with secondary antibodies coupled to Alexa dyes and rhodamine-phalloidin or phalloidin-Alexa-660 (all from Molecular Probes). After washing, samples were mounted in Vectashield containing DAPI. Images were acquired with a Zeiss LSM 780 confocal microscope and processed with Fiji (Schindelin et al., 2012) and Photoshop (Adobe).

Protein detection by Western blotting used standard procedures. 15 adult males were homogenised in 200 µl SDS buffer (250 mM Tris pH 6.8, 30 % glycerol, 1 % SDS, 500 mM DTT) and 5 µl were loaded per lane of a 10 % SDS-PAGE gel. The Immobilon membranes (Millipore) were blocked with 10 % milk powder and incubated with primary antibodies overnight (mouse anti-V5 1:10,000 (Invitrogen), mouse anti-Dlg1 1:10,000, rabbit anti-Mlp84B 1:20,000, rabbit anti-Fln 1:10,000). Detection used POD-coupled secondary antibodies (Jackson labs) and chemiluminescence (Millipore) using a LAS4000 detector system (FujiFilm).

Live imaging

889 SPIM imaging of embryos: De-chorionated embryos of the appropriate age were embedded
890 in 1 % low melting point agarose and mounted into a glass capillary. Fluorescent
891 microspheres (FY050 Estapor microspheres, Merck Millipore; 1:4000) were included in the
892 embedding medium for multi-view registration. The embryos were imaged using the Zeiss
893 Lightsheet Z.1 with a Zeiss 20x/1.0 water-immersion Plan Apochromat objective lens with
894 0.8x zoom at 25 °C using 488 nm laser set at 4 mW. Five views were imaged using dual-
895 sided illumination with Zeiss 10x/0.2 illumination lenses. A mean fusion was applied to
896 fuse both illumination sides after acquisition using the ZEN software (Zeiss). The views
897 were acquired at 72° angles with a stack size of 130 µm and a step size of 1.5 µm.
898 Exposure time were 30 ms per slice. Each slice consists of 1920 x 1200 pixels with a pixel
899 size of 0.29 µm and a bit depth of 16 bits. The light sheet thickness was 4 µm at the center
900 of the field of view. The embryos were imaged from onset of GFP expression (determined
901 empirically) until late embryogenesis with a time resolution of 15 min. Multi-view
902 processing of the dataset was carried out using the Fiji plugin for multi-view reconstruction
903 (Preibisch et al., 2009; Schmied et al., 2014), which was executed on a high performance
904 computing cluster (Schmied et al., 2015). The multi-view reconstruction was followed by
905 multi-view deconvolution (Preibisch et al., 2014), for which the images were down
906 sampled by a factor of two. Videos were extracted via the Fiji plugin BigDataViewer
907 (Pietzsch et al., 2015).
908 The Gsb-GFP fTRG line was crossed with the H2Av-mRFPruby line (Fischer et al., 2004;
909 Preibisch et al., 2014), the embryos of this cross were imaged using a 40x/1.0 water
910 immersion Plan Apochromat lens from Zeiss with 1x zoom at 25 °C at 17.5 mW of the 488
911 nm laser and 4 mW of the 561 nm laser. A single angle with dual sided illumination was
912 imaged. The stack size was 82.15 µm with a step size of 0.53 µm. Exposure time was 30
913 ms per slice. Each slice consisted of 1920 x 1920 pixels with a pixel size of 120 nm and a

914 bit depth of 16-bit. The light sheet thickness was 3.21 µm at the center of the field of view.
915 The embryos were imaged from early blastoderm onwards until late embryogenesis
916 focusing on the head with a time resolution of 7 min.
917 Imaging of pupae: Staging and live imaging of the pupae were performed at 27 ºC. Live
918 imaging of pupae at the appropriate stage was done as described previously (Weitkunat and
919 Schnorrer, 2014). Briefly, the staged pupa was cleaned with a brush and a small
920 observation window was cut into the pupal case with sharp forceps. The pupa was mounted
921 on a custom-made slide and the opening was covered with a small drop of 50 % glycerol
922 and a cover slip. Z-stacks of either single time points or long-term time-lapse Videos were
923 acquired using either a spinning disc confocal microscope (Zeiss, Visitron) or a two-photon
924 microscope (LaVision), both equipped with heated stages.
925
926 **Proteomics**
927 Per sample about hundred pupae or adult flies were snap-frozen in liquid nitrogen and
928 ground to a powder. The powder was re-suspended and further processed as described in
929 the quantitative BAC-GFP interactomics protocol (Hubner et al., 2010). In brief, 800 µl of
930 lysate per sample were cleared by centrifugation. The cleared lysate was mixed with
931 magnetic beads pre-coupled to anti-GFP antibodies and run over magnetic micro-columns
932 (both Miltenyi Biotec). Columns were washed, and samples subjected to in-column tryptic
933 digestion for 30 min. Eluates were collected and digestion continued overnight, followed
934 by desalting and storage on StageTips. Eluted peptides were analysed with an Orbitrap
935 mass spectrometer (Thermo Fisher). Raw data were analysed in MaxQuant version 1.4.3.22
936 (Cox and Mann, 2008) using the MaxLFQ algorithm for label-free quantification (Cox et
937 al., 2014). Interacting proteins were identified by the similarity of their intensity profiles to

938 the respective baits (Keilhauer et al., 2014). Heat maps were plotted in the Perseus module
939 of the MaxQuant software suite.
940
941 **Author contributions**
942 D.S., S.H., E.V. and M.S performed the liquid culture recombineering experiments.
943 M.S., S.J., P.K. and S.S. analysed the NGS data and contributed to the TransgeneOme
944 database.
945 B.S., N.P., K.F. and F.S performed the transgenesis of about half the fTRG lines.
946 V.K.J.V., R.T.K., K.A., M.R. and K.V performed the transgenesis of the other half of the
947 fTRG lines.
948 C.B. performed most of the genetic rescue experiments.
949 H.J. performed and analysed all experiments in ovaries.
950 C.S. collected and analysed SPIM in toto images of embryos.
951 C.B. and F.S. collected and analysed all imaging data in pupae and adults.
952 F.S. performed the Western blots of adult extracts.
953 M.Y.H and M.M. performed the proteomics analysis and analysed the data.
954 V.H. contributed analysis of Gsb-GFP cell tracking.
955 R.K.E. constructed the tagging cassettes.
956 I.R.S.F. performed initial proof of principle fosmid experiments in adult flies.
957 P.T. wrote the scripts to analyse *Drosophila* gene models.
958 P.T., F.S., M.S. and E.K. initiated the collaborative project and obtained dedicated funding.
959 P.T. and F.S. conceived and coordinated the study and co-wrote the manuscript with input
960 from the other authors.
961
962 **Acknowledgements**

Stocks obtained from the Bloomington *Drosophila* Stock Center (NIH P40OD018537) were used in this study. We are grateful to Belinda Bullard, Anne Ephrussi, Judith Saide, Jürgen Knoblich, Stefan Baumgartner, Kathleen Clark, Jim Vigoreaux and the DSHB for generously sharing antibodies and fly lines. We thank Franziska Friedrich for drawing the ovariole scheme used for Figure 3A. We thank Andreas Dahl from the Deep Sequencing Group at CRTD/BIOTECH, Dresden for the NGS library preparation and sequencing. We also thank the light microscopy facility and the computer department for assistance with imaging and data processing. We are grateful to Sandra Lemke, Aynur Kaya-Copur and Xu Zhang for help with the genetic rescue experiments and to Caroline Sonsteby for assistance during some of the pupal imaging experiments. We thank the entire Schnorrer lab for helpful comments on this manuscript. We are particularly grateful to Reinhard Fässler and Herbert Jäckle for continuous support of this work. This work was funded by the EMBO Young Investigator Program (F. S.) the European Research Council under the European Union's Seventh Framework Programme (FP/2007-2013)/ERC Grant 310939 (F. S.), the European Research Council under the European Union's Seventh Framework Programme (FP/2007-2013)/ERC Grant 260746 (P.T.), European Commission GENCODYS (P.T. and H.J.), Human Frontier Science Program (HFSP) RGY0093/2012 (P.T. and C. S.) and the Max Planck Society (P.T., F.S., M.S., M.M. and E.K.).

Competing interests

The authors declare that no competing interests exist.

References

Adams, M.D., Celniker, S.E., Holt, R.A., Evans, C.A., Gocayne, J.D., Amanatides, P.G., Scherer, S.E., Li, P.W., Hoskins, R.A., Galle, R.F., et al. (2000). The genome sequence of

Drosophila melanogaster. Science *287*, 2185–2195.

Baena-Lopez, L.A., Alexandre, C., Mitchell, A., Pasakarnis, L., and Vincent, J.P. (2013). Accelerated homologous recombination and subsequent genome modification in Drosophila. Development *140*, 4818–4825.

Bard, F., Casano, L., Mallabiabarrena, A., Wallace, E., Saito, K., Kitayama, H., Guizzunti, G., Hu, Y., Wendler, F., DasGupta, R., et al. (2006). Functional genomics reveals genes involved in protein secretion and Golgi organization. Nature *439*, 604–607.

Bischof, J., Bjorklund, M., Furger, E., Schertel, C., Taipale, J., and Basler, K. (2013). A versatile platform for creating a comprehensive UAS-ORFeome library in Drosophila. Development *140*, 2434–2442.

Bolatto, C., Chifflet, S., Megighian, A., and Cantera, R. (2003). Synaptic activity modifies the levels of Dorsal and Cactus at the neuromuscular junction of Drosophila. J. Neurobiol. *54*, 525–536.

Bonnay, F., Cohen-Berros, E., Hoffmann, M., Kim, S.Y., Boulianne, G.L., Hoffmann, J.A., Matt, N., and Reichhart, J.-M. (2013). big bang gene modulates gut immune tolerance in Drosophila. Proceedings of the National Academy of Sciences *110*, 2957–2962.

Bulgakova, N.A., and Knust, E. (2009). The Crumbs complex: from epithelial-cell polarity to retinal degeneration. Journal of Cell Science *122*, 2587–2596.

Buszczak, M., Paterno, S., Lighthouse, D., Bachman, J., Planck, J., Owen, S., Skora, A.D., Nystul, T.G., Ohlstein, B., Allen, A., et al. (2007). The carnegie protein trap library: a versatile tool for Drosophila developmental studies. Genetics *175*, 1505–1531.

Caussinus, E., Kanca, O., and Affolter, M. (2011). Fluorescent fusion protein knockout mediated by anti-GFP nanobody. Nat. Struct. Mol. Biol. *19*, 117–121.

Clark, K.A., Bland, J.M., and Beckerle, M.C. (2007). The Drosophila muscle LIM protein, Mlp84B, cooperates with D-titin to maintain muscle structural integrity. Journal of Cell Science *120*, 2066–2077.

Collins, K.A., Unruh, J.R., Slaughter, B.D., Yu, Z., Lake, C.M., Nielsen, R.J., Box, K.S., Miller, D.E., Blumenstiel, J.P., Perera, A.G., et al. (2014). Corolla is a novel protein that contributes to the architecture of the synaptonemal complex of Drosophila. Genetics *198*, 219–228.

Cox, J., and Mann, M. (2008). MaxQuant enables high peptide identification rates, individualized p.p.b.-range mass accuracies and proteome-wide protein quantification. Nature Biotechnology *26*, 1367–1372.

Cox, J., Hein, M.Y., Luber, C.A., Paron, I., Nagaraj, N., and Mann, M. (2014). Accurate proteome-wide label-free quantification by delayed normalization and maximal peptide ratio extraction, termed MaxLFQ. Mol. Cell Proteomics *13*, 2513–2526.

Cox, R.T., and Spradling, A.C. (2009). clueless, a conserved Drosophila gene required for mitochondrial subcellular localization, interacts genetically with parkin. Disease Models & Mechanisms *2*, 490–499.

1028 Cripps, R.M., Ball, E., Stark, M., Lawn, A., and Sparrow, J.C. (1994). Recovery of
1029 dominant, autosomal flightless mutants of Drosophila melanogaster and identification of a
1030 new gene required for normal muscle structure and function. Genetics *137*, 151–164.

1031 De Celis, J.F., Barrio, R., and Kafatos, F.C. (1999). Regulation of the spalt/spalt-related
1032 gene complex and its function during sensory organ development in the Drosophila thorax.
1033 Development *126*, 2653–2662.

1034 Deal, R.B., and Henikoff, S. (2010). A simple method for gene expression and chromatin
1035 profiling of individual cell types within a tissue. Developmental Cell *18*, 1030–1040.

1036 Dietzl, G., Chen, D., Schnorrer, F., Su, K.-C., Barinova, Y., Fellner, M., Gasser, B., Kinsey,
1037 K., Oppel, S., Scheiblauer, S., et al. (2007). A genome-wide transgenic RNAi library for
1038 conditional gene inactivation in Drosophila. Nature *448*, 151–156.

1039 Dougherty, G.W., Chopp, T., Qi, S.-M., and Cutler, M.L. (2005). The Ras suppressor Rsu-
1040 1 binds to the LIM 5 domain of the adaptor protein PINCH1 and participates in adhesion-
1041 related functions. Experimental Cell Research *306*, 168–179.

1042 Dunst, S., Kazimiers, T., Zadow, von, F., Jambor, H., Sagner, A., Brankatschk, B.,
1043 Mahmoud, A., Spannl, S., Tomancak, P., Eaton, S., et al. (2015). Endogenously tagged rab
1044 proteins: a resource to study membrane trafficking in Drosophila. Developmental Cell *33*,
1045 351–365.

1046 Ejsmont, R.K., Sarov, M., Winkler, S., Lipinski, K.A., and Tomancak, P. (2009). A toolkit
1047 for high-throughput, cross-species gene engineering in Drosophila. Nature Methods *6*, 435–
1048 437.

1049 Ejsmont, R.K., Ahlfeld, P., Pozniakovsky, A., Stewart, A.F., Tomancak, P., and Sarov, M.
1050 (2011). Recombination-mediated genetic engineering of large genomic DNA transgenes.
1051 Methods Mol. Biol. *772*, 445–458.

1052 Ephrussi, A., Dickinson, L.K., and Lehmann, R. (1991). Oskar organizes the germ plasm
1053 and directs localization of the posterior determinant nanos. Cell *66*, 37–50.

1054 Fernandes, J., Bate, M., and VijayRaghavan, K. (1991). Development of the indirect flight
1055 muscles of Drosophila. Development *113*, 67–77.

1056 Fernandes, J.J., Atreya, K.B., Desai, K.M., Hall, R.E., Patel, M.D., Desai, A.A., Benham,
1057 A.E., Mable, J.L., and Straessle, J.L. (2005). A dominant negative form of Rac1 affects
1058 myogenesis of adult thoracic muscles in Drosophila. Developmental Biology *285*, 11–27.

1059 Fessler, L.I., Campbell, A.G., Duncan, K.G., and Fessler, J.H. (1987). Drosophila laminin:
1060 characterization and localization. Journal of Cell Biology *105*, 2383–2391.

1061 Fischer, M., Haase, I., Simmeth, E., Gerisch, G., and Müller-Taubenberger, A. (2004). A
1062 brilliant monomeric red fluorescent protein to visualize cytoskeleton dynamics in
1063 Dictyostelium. FEBS Letters *577*, 227–232.

1064 Formstecher, E., Aresta, S., Collura, V., Hamburger, A., Meil, A., Trehin, A., Reverdy, C.,
1065 Betin, V., Maire, S., Brun, C., et al. (2005). Protein interaction mapping: a Drosophila case
1066 study. Genome Research *15*, 376–384.

1067 Forrest, K.M., and Gavis, E.R. (2003). Live imaging of endogenous RNA reveals a
1068 diffusion and entrapment mechanism for nanos mRNA localization in Drosophila. Current
1069 Biology *13*, 1159–1168.

1070 Garrison, E., and Marth, G. (1207). Haplotype-based variant detection from short-read
1071 sequencing. 2012.

1072 Gavin, A.-C., Bösche, M., Krause, R., Grandi, P., Marzioch, M., Bauer, A., Schultz, J.,
1073 Rick, J.M., Michon, A.-M., Cruciat, C.-M., et al. (2002). Functional organization of the
1074 yeast proteome by systematic analysis of protein complexes. Nature *415*, 141–147.

1075 Giot, L., Bader, J.S., Brouwer, C., Chaudhuri, A., Kuang, B., Li, Y., Hao, Y.L., Ooi, C.E.,
1076 Godwin, B., Vitols, E., et al. (2003). A protein interaction map of Drosophila melanogaster.
1077 Science *302*, 1727–1736.

1078 Gratz, S.J., Ukken, F.P., Rubinstein, C.D., Thiede, G., Donohue, L.K., Cummings, A.M.,
1079 and O'Connor-Giles, K.M. (2014). Highly specific and efficient CRISPR/Cas9-catalyzed
1080 homology-directed repair in Drosophila. Genetics *196*, 961–971.

1081 Graveley, B.R., Brooks, A.N., Carlson, J.W., Duff, M.O., Landolin, J.M., Yang, L., Artieri,
1082 C.G., van Baren, M.J., Boley, N., Booth, B.W., et al. (2011). The developmental
1083 transcriptome of Drosophila melanogaster. Nature *471*, 473–479.

1084 Guruharsha, K.G., Rual, J.-F., Zhai, B., Mintseris, J., Vaidya, P., Vaidya, N., Beekman, C.,
1085 Wong, C., Rhee, D.Y., Cenaj, O., et al. (2011). A Protein Complex Network of Drosophila
1086 melanogaster. Cell *147*, 690–703.

1087 Gutjahr, T., Patel, N.H., Li, X., Goodman, C.S., and Noll, M. (1993). Analysis of the
1088 gooseberry locus in Drosophila embryos: gooseberry determines the cuticular pattern and
1089 activates gooseberry neuro. Development *118*, 21–31.

1090 Haecker, A., Bergman, M., Neupert, C., Moussian, B., Luschnig, S., Aebi, M., and
1091 Mannervik, M. (2008). Wollknauel is required for embryo patterning and encodes the
1092 Drosophila ALG5 UDP-glucose:dolichyl-phosphate glucosyltransferase. Development *135*,
1093 1745–1749.

1094 Hammonds, A.S., Bristow, C.A., Fisher, W.W., Weiszmann, R., Wu, S., Hartenstein, V.,
1095 Kellis, M., Yu, B., Frise, E., and Celniker, S.E. (2013). Spatial expression of transcription
1096 factors in Drosophila embryonic organ development. Genome Biology *14*, R140.

1097 Hartenstein, V., Younossi-Hartenstein, A., Lovick, J.K., Kong, A., Omoto, J.J., Ngo, K.T.,
1098 and Viktorin, G. (2015). Lineage-associated tracts defining the anatomy of the Drosophila
1099 first instar larval brain. Developmental Biology *406*, 14–39.

1100 He, H., and Noll, M. (2013). Differential and redundant functions of gooseberry and
1101 gooseberry neuro in the central nervous system and segmentation of the Drosophila embryo.
1102 Developmental Biology *382*, 209–223.

1103 Hein, M.Y., Hubner, N.C., Poser, I., Cox, J., Nagaraj, N., Toyoda, Y., Gak, I.A.,
1104 Weisswange, I., Mansfeld, J., Buchholz, F., et al. (2015). A Human Interactome in Three
1105 Quantitative Dimensions Organized by Stoichiometries and Abundances. Cell *163*, 712–
1106 723.

Ho, Y., Gruhler, A., Heilbut, A., Bader, G.D., and Moore, L. (2002). Systematic identification of protein complexes in Saccharomyces cerevisiae by mass spectrometry. Nature *415*, 180–183.

Hofemeister, H., Ciotta, G., Fu, J., Seibert, P.M., Schulz, A., Maresca, M., Sarov, M., Anastassiadis, K., and Stewart, A.F. (2011). Recombineering, transfection, Western, IP and ChIP methods for protein tagging via gene targeting or BAC transgenesis. Methods *53*, 437–452.

Hubner, N.C., Bird, A.W., Cox, J., Splettstoesser, B., Bandilla, P., Poser, I., Hyman, A., and Mann, M. (2010). Quantitative proteomics combined with BAC TransgeneOmics reveals in vivo protein interactions. The Journal of Cell Biology *189*, 739–754.

Huisken, J., and Stainier, D.Y.R. (2007). Even fluorescence excitation by multidirectional selective plane illumination microscopy (mSPIM). Opt Lett *32*, 2608–2610.

Huisken, J., Swoger, J., Del Bene, F., Wittbrodt, J., and Stelzer, E.H.K. (2004). Optical sectioning deep inside live embryos by selective plane illumination microscopy. Science *305*, 1007–1009.

Hutterer, A., Betschinger, J., Petronczki, M., and Knoblich, J.A. (2004). Sequential roles of Cdc42, Par-6, aPKC, and Lgl in the establishment of epithelial polarity during Drosophila embryogenesis. Developmental Cell *6*, 845–854.

Izumi, Y., Yanagihashi, Y., and Furuse, M. (2012). A novel protein complex, Mesh-Ssk, is required for septate junction formation in the Drosophila midgut. Journal of Cell Science *125*, 4923–4933.

Jambor, H., Brunel, C., and Ephrussi, A. (2011). Dimerization of oskar 3' UTRs promotes hitchhiking for RNA localization in the Drosophila oocyte. Rna *17*, 2049–2057.

Jambor, H., Mueller, S., Bullock, S.L., and Ephrussi, A. (2014). A stem-loop structure directs oskar mRNA to microtubule minus ends. Rna *20*, 429–439.

Jambor, H., Surendranath, V., Kalinka, A.T., Mejstrik, P., Saalfeld, S., and Tomancak, P. (2015). Systematic imaging reveals features and changing localization of mRNAs in Drosophila development. eLife *4*, e05003.

Jiang, H., and Edgar, B.A. (2011). Intestinal stem cells in the adult Drosophila midgut. Experimental Cell Research *317*, 2780–2788.

Kadrmas, J.L., Smith, M.A., Clark, K.A., Pronovost, S.M., Muster, N., Yates, J.R., and Beckerle, M.C. (2004). The integrin effector PINCH regulates JNK activity and epithelial migration in concert with Ras suppressor 1. Journal of Cell Biology *167*, 1019–1024.

Katzemich, A., Kreisköther, N., Alexandrovich, A., Elliott, C., Schöck, F., Leonard, K., Sparrow, J., and Bullard, B. (2012). The function of the M-line protein obscurin in controlling the symmetry of the sarcomere in the flight muscle of Drosophila. Journal of Cell Science *125*, 3367–3379.

Keilhauer, E.C., Hein, M.Y., and Mann, M. (2014). Accurate Protein Complex Retrieval by Affinity Enrichment Mass Spectrometry (AE-MS) Rather than Affinity Purification Mass

Spectrometry (AP-MS). Molecular & Cellular Proteomics *14*, 120–135.

Kim-Ha, J., Kerr, K., and Macdonald, P.M. (1995). Translational regulation of oskar mRNA by bruno, an ovarian RNA-binding protein, is essential. Cell *81*, 403–412.

Kim-Ha, J., Smith, J.L., and Macdonald, P.M. (1991). oskar mRNA is localized to the posterior pole of the Drosophila oocyte. Cell *66*, 23–35.

Krogan, N.J., Cagney, G., Yu, H., Zhong, G., Guo, X., Ignatchenko, A., Li, J., Pu, S., Datta, N., Tikuisis, A.P., et al. (2006). Global landscape of protein complexes in the yeast Saccharomyces cerevisiae. Nature *440*, 637–643.

Kvon, E.Z., Kazmar, T., Stampfel, G., Yáñez-Cuna, J.O., Pagani, M., Schernhuber, K., Dickson, B.J., and Stark, A. (2014). Genome-scale functional characterization of Drosophila developmental enhancers in vivo. Nature *512*, 91–95.

Langmead, B., and Salzberg, S.L. (2012). Fast gapped-read alignment with Bowtie 2. Nature Methods *9*, 357–359.

Leiss, D., Hinz, U., Gasch, A., Mertz, R., and Renkawitz-Pohl, R. (1988). Beta 3 tubulin expression characterizes the differentiating mesodermal germ layer during Drosophila embryogenesis. Development *104*, 525–531.

Lécuyer, E., Yoshida, H., Parthasarathy, N., Alm, C., Babak, T., Cerovina, T., Hughes, T.R., Tomancak, P., and Krause, H.M. (2007). Global analysis of mRNA localization reveals a prominent role in organizing cellular architecture and function. Cell *131*, 174–187.

Li, H., Handsaker, B., Wysoker, A., Fennell, T., Ruan, J., Homer, N., Marth, G., Abecasis, G., Durbin, R., 1000 Genome Project Data Processing Subgroup (2009). The Sequence Alignment/Map format and SAMtools. Bioinformatics *25*, 2078–2079.

Lovick, J.K., Ngo, K.T., Omoto, J.J., Wong, D.C., Nguyen, J.D., and Hartenstein, V. (2013). Postembryonic lineages of the Drosophila brain_ I. Development of the lineage-associated fiber tracts. Developmental Biology *384*, 228–257.

Lowe, N., Rees, J.S., Roote, J., Ryder, E., Armean, I.M., Johnson, G., Drummond, E., Spriggs, H., Drummond, J., Magbanua, J.P., et al. (2014). Analysis of the expression patterns, subcellular localisations and interaction partners of Drosophila proteins using a pigP protein trap library. Development *141*, 3994–4005.

Meacock, P.A., and Cohen, S.N. (1980). Partitioning of bacterial plasmids during cell division: a cis-acting locus that accomplishes stable plasmid inheritance. Cell *20*, 529–542.

Metcalf, W.W., Jiang, W., Daniels, L.L., Kim, S.K., Haldimann, A., and Wanner, B.L. (1996). Conditionally replicative and conjugative plasmids carrying lacZ alpha for cloning, mutagenesis, and allele replacement in bacteria. Plasmid *35*, 1–13.

Morin, X., Daneman, R., Zavortink, M., and Chia, W. (2001). A protein trap strategy to detect GFP-tagged proteins expressed from their endogenous loci in Drosophila. Proceedings of the National Academy of Sciences of the United States of America *98*, 15050–15055.

1184 Nagarkar-Jaiswal, S., Lee, P.-T., Campbell, M.E., Chen, K., Anguiano-Zarate, S., Gutierrez,
1185 M.C., Busby, T., Lin, W.-W., He, Y., Schulze, K.L., et al. (2015). A library of MiMICs
1186 allows tagging of genes and reversible, spatial and temporal knockdown of proteins in
1187 Drosophila. eLife *4*.

1188 Neuman-Silberberg, F.S., and Schüpbach, T. (1993). The Drosophila dorsoventral
1189 patterning gene gurken produces a dorsally localized RNA and encodes a TGF alpha-like
1190 protein. Cell *75*, 165–174.

1191 Neumuller, R.A., Wirtz-Peitz, F., Lee, S., Kwon, Y., Buckner, M., Hoskins, R.A., Venken,
1192 K.J.T., Bellen, H.J., Mohr, S.E., and Perrimon, N. (2012). Stringent Analysis of Gene
1193 Function and Protein-Protein Interactions Using Fluorescently Tagged Genes. Genetics *190*,
1194 931–940.

1195 Ni, J.-Q., Zhou, R., Czech, B., Liu, L.-P., Holderbaum, L., Yang-Zhou, D., Shim, H.-S.,
1196 Tao, R., Handler, D., Karpowicz, P., et al. (2011). A genome-scale shRNA resource for
1197 transgenic RNAi in Drosophila. Nature Methods *8*, 405–407.

1198 Nongthomba, U., Pasalodos-Sanchez, S., Clark, S., Clayton, J., and Sparrow, J. (2001).
1199 Expression and function of the Drosophila ACT88F actin isoform is not restricted to the
1200 indirect flight muscles. J Muscle Res Cell Motil *22*, 111–119.

1201 Oas, S.T., Bryantsev, A.L., and Cripps, R.M. (2014). Arrest is a regulator of fiber-specific
1202 alternative splicing in the indirect flight muscles of Drosophila. The Journal of Cell
1203 Biology *206*, 895–908.

1204 Ohlstein, B., and Spradling, A. (2005). The adult Drosophila posterior midgut is
1205 maintained by pluripotent stem cells. Nature *439*, 470–474.

1206 Pereanu, W. (2006). Neural Lineages of the Drosophila Brain: A Three-Dimensional
1207 Digital Atlas of the Pattern of Lineage Location and Projection at the Late Larval Stage.
1208 Journal of Neuroscience *26*, 5534–5553.

1209 Pédelacq, J.-D., Cabantous, S., Tran, T., Terwilliger, T.C., and Waldo, G.S. (2005).
1210 Engineering and characterization of a superfolder green fluorescent protein. Nature
1211 Biotechnology *24*, 79–88.

1212 Pietzsch, T., Saalfeld, S., Preibisch, S., and Tomancak, P. (2015). BigDataViewer:
1213 visualization and processing for large image data sets. Nature Methods *12*, 481–483.

1214 Port, F., Chen, H.-M., Lee, T., and Bullock, S.L. (2014). Optimized CRISPR/Cas tools for
1215 efficient germline and somatic genome engineering in Drosophila. Proceedings of the
1216 National Academy of Sciences *111*, E2967–E2976.

1217 Preibisch, S., Amat, F., Stamataki, E., Sarov, M., Singer, R.H., Myers, E., and Tomancak,
1218 P. (2014). Efficient Bayesian-based multiview deconvolution. Nature Methods *11*, 645–648.

1219 Preibisch, S., Saalfeld, S., and Tomancak, P. (2009). Globally optimal stitching of tiled 3D
1220 microscopic image acquisitions. Bioinformatics *25*, 1463–1465.

1221 Quiñones-Coello, A.T., Petrella, L.N., Ayers, K., Melillo, A., Mazzalupo, S., Hudson,
1222 A.M., Wang, S., Castiblanco, C., Buszczak, M., Hoskins, R.A., et al. (2007). Exploring

strategies for protein trapping in Drosophila. Genetics *175*, 1089–1104.

Razzaq, A., Robinson, I., McMahon, H., Skepper, J., Su, Y., Zelhof, A., Jackson, A., Gay, N., and O'Kane, C. (2001). Amphiphysin is necessary for organization of the excitation–contraction coupling machinery of muscles, but not for synaptic vesicle endocytosis in Drosophila. Genes & Development *15*, 2967.

Rørth, P. (1998). Gal4 in the Drosophila female germline. Mechanisms of Development *78*, 113–118.

Rørth, P., Szabo, K., Bailey, A., Laverty, T., Rehm, J., Rubin, G.M., Weigmann, K., Milán, M., Benes, V., Ansorge, W., et al. (1998). Systematic gain-of-function genetics in Drosophila. Development *125*, 1049–1057.

Sarov, M., Murray, J.I., Schanze, K., Pozniakovski, A., Niu, W., Angermann, K., Hasse, S., Rupprecht, M., Vinis, E., Tinney, M., et al. (2012). A genome-scale resource for in vivo tag-based protein function exploration in C. elegans. Cell *150*, 855–866.

Schertel, C., Albarca, M., Rockel-Bauer, C., Kelley, N.W., Bischof, J., Hens, K., van Nimwegen, E., Basler, K., and Deplancke, B. (2015). A large-scale, in vivo transcription factor screen defines bivalent chromatin as a key property of regulatory factors mediating Drosophila wing development. Genome Research *25*, 514–523.

Schindelin, J., Arganda-Carreras, I., Frise, E., Kaynig, V., Longair, M., Pietzsch, T., Preibisch, S., Rueden, C., Saalfeld, S., Schmid, B., et al. (2012). Fiji: an open-source platform for biological-image analysis. Nature Methods *9*, 676–682.

Schmied, C., Stamataki, E., and Tomancak, P. (2014). Open-source solutions for SPIMage processing. Methods Cell Biol. *123*, 505–529.

Schmied, C., Steinbach, P., Pietzsch, T., Preibisch, S., and Tomancak, P. (2015). An automated workflow for parallel processing of large multiview SPIM recordings. Bioinformatics btv706.

Schnorrer, F., Kalchhauser, I., and Dickson, B. (2007). The transmembrane protein Kon-tiki couples to Dgrip to mediate myotube targeting in Drosophila. Developmental Cell *12*, 751–766.

Schnorrer, F., Schönbauer, C., Langer, C.C.H., Dietzl, G., Novatchkova, M., Schernhuber, K., Fellner, M., Azaryan, A., Radolf, M., Stark, A., et al. (2010). Systematic genetic analysis of muscle morphogenesis and function in Drosophila. Nature *464*, 287–291.

Schönbauer, C., Distler, J., Jährling, N., Radolf, M., Dodt, H.-U., Frasch, M., and Schnorrer, F. (2011). Spalt mediates an evolutionarily conserved switch to fibrillar muscle fate in insects. Nature *479*, 406–409.

Sokolovski, M., Bhattacherjee, A., Kessler, N., Levy, Y., and Horovitz, A. (2015). Thermodynamic Protein Destabilization by GFP Tagging: A Case of Interdomain Allostery. Biophysical Journal *109*, 1157–1162.

Spletter, M.L., and Schnorrer, F. (2014). Transcriptional regulation and alternative splicing cooperate in muscle fiber-type specification in flies and mammals. Experimental Cell

Research *321*, 90–98.

Spletter, M.L., Barz, C., Yeroslaviz, A., Schönbauer, C., Ferreira, I.R.S., Sarov, M., Gerlach, D., Stark, A., Habermann, B.H., and Schnorrer, F. (2015). The RNA-binding protein Arrest (Bruno) regulates alternative splicing to enable myofibril maturation in Drosophila flight muscle. EMBO Rep *16*, 178–191.

St Johnston, D. (2012). Using mutants, knockdowns, and transgenesis to investigate gene function in Drosophila. WIREs Dev Biol *2*, 587–613.

Stadler, C., Rexhepaj, E., Singan, V.R., Murphy, R.F., Pepperkok, R., Uhlen, M., Simpson, J.C., and Lundberg, E. (2013). Immunofluorescence and fluorescent-protein tagging show high correlation for protein localization in mammalian cells. Nature Methods *10*, 315–323.

Sun, B., Xu, P., and Salvaterra, P.M. (1999). Dynamic visualization of nervous system in live Drosophila. Proceedings of the National Academy of Sciences of the United States of America *96*, 10438–10443.

Tomancak, P., Beaton, A., Weiszmann, R., Kwan, E., Shu, S., Lewis, S.E., Richards, S., Ashburner, M., Hartenstein, V., Celniker, S.E., et al. (2002). Systematic determination of patterns of gene expression during Drosophila embryogenesis. Genome Biology *3*, RESEARCH0088.

Tomancak, P., Berman, B.P., Beaton, A., Weiszmann, R., Kwan, E., Hartenstein, V., Celniker, S.E., and Rubin, G.M. (2007). Global analysis of patterns of gene expression during Drosophila embryogenesis. Genome Biology *8*, R145.

Tracey, W.D., Wilson, R.I., Laurent, G., and Benzer, S. (2003). painless, a Drosophila gene essential for nociception. Cell *113*, 261–273.

Trcek, T., Grosch, M., York, A., Shroff, H., Lionnet, T., and Lehmann, R. (2015). Drosophila germ granules are structured and contain homotypic mRNA clusters. Nature Communications *6*, 7962.

Tseng, A.-S.K., and Hariharan, I.K. (2002). An overexpression screen in Drosophila for genes that restrict growth or cell-cycle progression in the developing eye. Genetics *162*, 229–243.

Tu, Y., Huang, Y., Zhang, Y., Hua, Y., and Wu, C. (2001). A new focal adhesion protein that interacts with integrin-linked kinase and regulates cell adhesion and spreading. Journal of Cell Biology *153*, 585–598.

Vaskova, M., Bentley, A.M., Marshall, S., Reid, P., Thummel, C.S., and Andres, A.J. (2000). Genetic analysis of the Drosophila 63F early puff. Characterization of mutations in E63-1 and maggie, a putative Tom22. Genetics *156*, 229–244.

Venken, K.J.T., and Bellen, H.J. (2012). Genome-Wide Manipulations of Drosophila melanogaster with Transposons, Flp Recombinase, and ΦC31 Integrase. Methods Mol. Biol. *859*, 203–228.

Venken, K.J.T., Carlson, J.W., Schulze, K.L., Pan, H., He, Y., Spokony, R., Wan, K.H., Koriabine, M., de Jong, P.J., White, K.P., et al. (2009). Versatile P[acman] BAC libraries

1301 for transgenesis studies in Drosophila melanogaster. Nature Methods *6*, 431–434.

1302 Venken, K.J.T., He, Y., Hoskins, R.A., and Bellen, H.J. (2006). P[acman]: a BAC
1303 transgenic platform for targeted insertion of large DNA fragments in D. melanogaster.
1304 Science *314*, 1747–1751.

1305 Venken, K.J.T., Popodi, E., Holtzman, S.L., Schulze, K.L., Park, S., Carlson, J.W., Hoskins,
1306 R.A., Bellen, H.J., and Kaufman, T.C. (2010). A molecularly defined duplication set for the
1307 X chromosome of Drosophila melanogaster. Genetics *186*, 1111–1125.

1308 Venken, K.J.T., Schulze, K.L., Haelterman, N.A., Pan, H., He, Y., Evans-Holm, M.,
1309 Carlson, J.W., Levis, R.W., Spradling, A.C., Hoskins, R.A., et al. (2011). MiMIC: a highly
1310 versatile transposon insertion resource for engineering Drosophila melanogaster genes.
1311 Nature Methods *8*, 737–743.

1312 Vernes, S.C. (2014). Genome wide identification of fruitless targets suggests a role in
1313 upregulating genes important for neural circuit formation. Sci Rep *4*, 4412.

1314 Vigoreaux, J., Saide, J., Valgeirsdottir, K., and Pardue, M. (1993). Flightin, a novel
1315 myofibrillar protein of Drosophila stretch-activated muscles. Journal of Cell Biology *121*,
1316 587.

1317 Wangler, M.F., Yamamoto, S., and Bellen, H.J. (2015). Fruit flies in biomedical research.
1318 Genetics *199*, 639–653.

1319 Weitkunat, M., and Schnorrer, F. (2014). A guide to study Drosophila muscle biology.
1320 Methods *68*, 2–14.

1321 Weitkunat, M., Kaya-Copur, A., Grill, S.W., and Schnorrer, F. (2014). Tension and force-
1322 resistant attachment are essential for myofibrillogenesis in Drosophila flight muscle. Curr
1323 Biol *24*, 705–716.

1324 Younossi-Hartenstein, A., Salvaterra, P.M., and Hartenstein, V. (2002). Early development
1325 of theDrosophila brain: IV. Larval neuropile compartments defined by glial septa. The
1326 Journal of Comparative Neurology *455*, 435–450.

1327 Zhang, X., Koolhaas, W.H., and Schnorrer, F. (2014). A versatile two-step CRISPR-and
1328 RMCE-based strategy for efficient genome engineering in Drosophila. G3 (Bethesda) *4*,
1329 2409–2418.

1330

Figure 1. Generation of the TransgeneOme library

(A) Overview of the tagging strategy. Liquid culture recombineering is used to insert a 'pre-tagging' cassette into FlyFos genomic clones in bacteria. This cassette can then be replaced by a simple, universal, recombineering reaction with any tag of choice, here, a superfolder GFP tag (sGFP) to generate the sGFP TransgeneOme clone library. These clones are transformed into flies generating transgenic FlyFos libraries that can be used for multiple *in vivo* applications.

(**B**) TransgeneOme resource engineering. The steps of the recombineering pipeline are shown on the left with the success rate of each step indicated on the right (red colour denotes bacterial clones that did not grow). The *E. coli* cells are schematically represented with a dotted circle. With the first two steps the 'pre-tagging' cassette is inserted, which is replaced in the next three steps with the sGFP cassette to generate the sGFP TransgeneOme library. See text and methods section for details; abbreviations: *GoI* – gene of interest; *cat* – chloramphenicol resistance gene, F-ori – the fosmid vector replication control sequences; pRedFlp – recombineering helper plasmid with the pSC101 temperature sensitive origin of replication, which can be maintained at 30 ºC and is removed at the final step by temperature shift to 37 ºC; it carries the Red gbaA operon (Red), which drives homologous recombination *in vivo*, under the control of the L-Rhamnose (Rham) inducible promoter (rhaP) and the Flp recombinase (Flp) under the control of tetracycline (Tet) inducible promoter (tetP); pretag – a pre-tagging cassette consisting of the Nourseothricin resistance gene (nat), flanked by the 2xTY and 3xFlag tag, which provide regions of homology to the tagging cassette (tag), consisting of the TY1 tag, superfolder GFP (sGFP), the V5 tag and the target peptide for the birA biotin ligase (blrp), the FRT-flanked selection/counter-selection operon rpsl-neo (confers streptomycin sensitivity and kanamycin resistance) and the 3xFlag tag. (**C**) Next-generation-sequencing (NGS)-based validation of the sGFP

TransgeneOme library. Schematic of the bar coding (BC) strategy of row and column pools is shown to the left and sequencing results to the right. In this example, a clone with the coordinates A1 will receive the row A barcode (blue) and the column 1 barcode (yellow), which allow the mapping of the NGS sequence reads to the respective well. By using the mate-paired strategy the reads mapping to the tag can be assigned to a specific transgene, i.e. only reads where one mate of the pair maps to the tag and the other to the genome are used. Sequenced tags within fosmids without point mutations are shown in solid green, clones without mutation in tagging cassette but incomplete coverage in light green and clones with mutation(s) or un-flipped cassette are shown in red. (**D**) Statistics of the mutation distributions with deletions indicated by green, substitutions by red and insertions by blue interrupted lines. Note that most mutations reside within the recombineering primer sequences (denoted as black arrows).

Figure 1 -figure supplement 1: Tagging cassettes

Tags tested and used in this study. Shown is the form of the tagging cassette after insertion into the target site and flip-out of the counter selection sequences (rpsl-neo) leaving behind the FRT sequence coloured in red. While both the TY1-sGFP-FLAG and TY1-sGFP-V5-BLRP-FLAG tags can be used for localisation of the tagged protein of interest *in vivo,* the latter offers additional affinity purification options and was the tag used for the genome-wide resource. The TY1-T2A-sGFPnls-FLAG results in cleavage at the T2A peptide and nuclear localization of the released sGFP-NLS fragment. Abbreviations: 2xTY1, 3xFlag, V5, Strep – epitope tags; BLRP – target peptide for the birA biotin ligase, allowing for tissue specific labelling and purification (through tissue specific expression of birA); Pre (Prescission protease) and TEV (Tobacco Etch Virus endopeptidase) cleavage sites; T2A - "self-cleaving" peptide; NLS – nuclear localization signal. The "pre-tagging" cassette can

be easily exchanged to any of the tagging cassettes through homologous recombination as it starts and ends with the same epitope tag encoding sequences.

Figure 2: Functionality tests of the GFP-tagged fTRG lines by genetic complementation analysis

(**A**) Genetic rescue statistics of null/strong mutant alleles for 46 selected fTRG lines. Note that more than two-thirds of the lines show a rescue (see **Table 2**). (**B**, **C**) *osk*-GFP mRNA (in yellow) expressed from fTRG1394 rescues egg-chamber development of an *osk* null allele (Jenny et al., 2006). *osk*-GFP mRNA enriches in the early oocyte (**B**, stage 6) and rescues the oogenesis arrest and the DNA condensation defect of the *osk* mutant (**B'**, yellow arrowhead). At stage 10 *osk*-GFP RNA enriches at the posterior pole (**C**) and produces sufficient protein to ensure proper embryogenesis. *osk*-GFP mRNA is shown in yellow, DAPI in magenta; scale bars indicate 30 µm.

Figure 3: Expression of fTRG tagged proteins in ovaries

(**A**) Schematic overview of oogenesis stages and cell types. (**B**) Summary of the identified expression patterns; see also **Supplementary File 3**. (**C**) Selected examples for cell type specific fTRG expression patterns at germarium, early- and mid-oogenesis stages visualised by anti-GFP antibody staining. (**D**) Selected examples of subcellular localisation patterns, highlighting nuclear, cortical and cytoplasmic patterns at different oogenesis stages. GFP is show in green, DAPI in magenta; scale bars indicate 30 µm.

Figure 3 -figure supplement 1: Co-localisation of fTRG derived tagged proteins with endogenous proteins during oogenesis

(**A**, **B**) Endogenous untagged Grk protein detected with an anti-Grk antibody localises similarly in wild-type stage 8 oocytes (**A**), as in fTRG960 oocytes expressing Grk-GFP

detected by an anti-GFP antibody (**B**). Note that both Grk and GFP antibody patterns are indistinguishable (compare **B** and **B'**). (**C**, **D**) Osk protein detected by an anti-Osk antibody in wild type stage 9 - 10 oocytes (**C**) compared to Osk antibody labelled protein in an fTRG1394 oocyte expressing Osk-GFP in addition to endogenous Osk (**D**). Note the co-localisation of anti-Osk and anti-GFP antibodies (**D** and **D'**). Scale bars indicate 30 µm.

Figure 3 -figure supplement 2: Posttranscriptional regulation of protein expression during oogenesis

(**A**, **B**) *osk-GFP* mRNA visualised by an anti-GFP labelled RNA probe (yellow, DAPI in magenta) at stage 6 and stage 10 of oogenesis. (**A**', **B**') Osk-GFP protein visualised by anti-GFP antibody (green, DAPI in magenta) at stage 6 and stage 10. Note that Osk-GFP protein is not detectable at stage 6. (**C, D**) *corolla-GFP* mRNA (yellow, DAPI in magenta) at stage 6 and stage 8. (**E, F**) Corolla-GFP protein (green, DAPI in magenta) at stage 6 and stage 8. Note that Corolla-GFP protein is only detectable at stage 6 but not stage 8. Scale bars indicate 30 µm.

Figure 4: Live *in toto* imaging during embryogenesis with SPIM

(**A** - **C**) Nrv2-GFP protein is enriched in cell membrane of the epidermis and the CNS of late stage 16 embryos, as shown by a lateral section (**A**) and high magnifications of the posterior epidermis (**B**) and the ventral CNS (**C**). (**D**) Schemes of the lateral, ventral and transverse optical section views through the embryo shown in (**E** - **I**). (**E** - **I**) Still image from a Nrv2-GFP time-lapse Video with lateral section views on the left, ventral sections in the middle and transverse sections on the right. Note that Nrv2-GFP is first expressed in the

developing epidermal epithelial cells (**E, F**) and then becomes enriched in the CNS (**G - I**, see **Video 1**). Scale bars indicate 50 µm.

Figure 4 -figure supplement 1: Live Gsb-GFP imaging during embryogenesis with SPIM

(**A**, **B**) Lateral view of a live stage 10 embryo expressing Gsb-GFP (green in A) and Histone2A-mRFPruby (red in A); anterior is to the left (see **Video 2**). (**C - F**) Confocal sections of *gsb*-positive deuterocerebral proneural domain (recorded with a regular confocal microscope at a similar position as boxed in **B**). Fate of cells is symbolized by different colours (blue: epidermal precursor undergoing no further mitosis; purple: epidermal precursor undergoing one mitosis; red: neuroblasts). (**C**) and (**D**) show an optical section through the neurectoderm of stage 10 embryo prior to neuroblast delamination; (**E**) and (**F**) display the same region 30 minutes later, after neuroblasts have delaminated (stage 11), with a superficial optical section of surface ectoderm (**E**), and deep section of the neuroblast layer (**F**). (**G - I**) Optical cross sections (rotated by 90 degrees) of a similar embryo as in (**A**) expressing GFP-tagged Gsb (green) and Histone-2A-mRFPruby (red) at stage 10 (**G**), early 11 (**H**) and late 11 (**I**) showing neuroblasts delaminating from Gsb-GFP domain. (**J**) Schematic cross section of stage 10 (left) and stage 11 (right) ectoderm illustrating fate of cells forming part of Gsb-positive pro-neural domain. Scale bars indicate 25µm (**A**, **B**) and 10 µm (**G - I**).

Figure 4 -figure supplement 2: Live Gsb-n-GFP imaging during embryogenesis with SPIM

(**A, B**). Ventral view of Gsb-n-GFP expression of a stage 12 embryo during germ-band retraction (**A**) and stage 14 during head involution (**B)**. Note that Gsb-n-GFP remains expressed in neuronal precursors during stage 14 (**Video 3**). Scale bars indicate 50 μm.

Figure 5: Expression of fTRG tagged proteins in tissues of the adult thorax.

Antibody stainings of the adult thorax with anti-GFP antibody (green) and phalloidin (red). (**A - F**) Act88-GFP expression is specific to the IFMs, where it labels the thin filaments (**B**), whereas Mlp84B specifically labels the Z-discs of leg muscles (**F**). (**G - J**) Tango1-GFP concentrates in a vesicle-like pattern in the gut epithelium (**H, H'**), whereas Par6-GFP is highly expressed in trachea (**I**) and the gut epithelium, where it concentrates at the apical membrane, as shown for a cross-section of the proventriculus (**J, J'**), nuclei are labelled with DAPI (blue). (**K - M**) Pain-GFP expression in the flight muscle motor neurons (**K**), small cells within the midgut epithelium (**L, L'**) and tendon cells (**M, M'**). (**N - P**) LanB1-GFP labels the extracellular matrix surrounding the IFMs, the motor neurons and the trachea (**N**), as well as the visceral muscles (**O**). Even the finest trachea marked by UV auto-fluorescence (white) (**P**) are surrounded by LanB1-GFP (**P'**). (**Q**) Pain-GFP positive cells in the midgut do not overlap with Prospero positive nuclei of enterocytes (in red) and contain small nuclei, as visualised by DAPI co-stain in white (**Q - Q'''**). Scale bars indicate 100 μm (**A**, **D**, **I**, **K**, **N**), 20 μm (**H**, **J**, **L**, **O, Q**) and 5 μm (**B**, **C**, **E**, **F**, **M**, **P**).

Figure 5 -figure supplement 1: Extracellular matrix and synaptic markers of the adult thorax.

(**A - H**) Antibody stainings of the adult thorax with anti-GFP antibody (green or white in the single colour images) and phalloidin (red). LanA-GFP and BM-40-SPARC-GFP labels the ECM around motor neurons, visceral muscle and trachea. Note that thin trachea within

1478 the IFMs (marked by UV auto-fluorescence in white) are surrounded by LanA-GFP but not
1479 BM-40-SPARC-GFP (**D**, **H**). (**I - M**) Cact-GFP (green) shows a distinct localisation in
1480 IFMs, leg and visceral muscle reminiscent of a neuromuscular junction pattern. Note the
1481 partial co-localisation with the motor neuron marker Futsch (in red, **M, M'**), whereas no
1482 co-localisation with trachea in IFMs (in white, **M**). Scale bars indicate 100 µm (**A**, **E**, **I**), 20
1483 µm (**B**, **C**, **F**, **G**, **L**), 10 µm (**M**) and 5 µm (**D**, **H**, **J**, **K**).
1484
1485 **Figure 6: Subcellular expression patterns in adult flight muscles**
1486 Antibody stainings of the adult thorax with anti-GFP antibody (green or white in the single
1487 colour images) and phalloidin (red). (**A - D**) Localisation to specific myofibrillar sub-
1488 regions; Fln-GFP marks the thick filaments (**A**, **A'**), Fray-GFP surrounds the myofibrils
1489 with an enrichment at M-lines and Z-discs (**B**, **B'**), Unc-89-GFP marks only M-lines (**C**,
1490 **C'**) and CG31772-GFP only Z-discs (**D**, **D'**). (**E - H**) Ilk-GFP strongly concentrates at the
1491 muscle-tendon attachment sites (**E**, **E'**), Dlg1-GFP labels the T-tubular membranes (**F**, **F'**),
1492 Babo-GFP shows a dotty, vesicular pattern (**G, G'**) and CG12118-GFP displays a
1493 mitochondrial pattern (**H**, **H'**). Scale bars indicate 5 µm.
1494
1495 **Figure 6 -figure supplement 1: CG12118-GFP localises to mitochondria**
1496 Co-staining of adult IFMs from fTRG276 (CG12118-GFP) with anti-GFP antibody (green)
1497 and the mitochondrial marker anti-complex V α (ATPase Vα, in red). Note the strong
1498 overlap of both signals. Scale bar indicate 5 µm.
1499
1500 **Figure 6 -figure supplement 2: Nuclear localisations in adult flight muscles**
1501 Antibody stainings of the adult thorax with anti-GFP antibody (green or white in the single
1502 colour images), phalloidin (red) and DAPI (blue). (**A - H**) CG11617-GFP (**A**, **E**),

CG12391-GFP (**B**, **F**) and CG17912 (**C**, **G**) are localised to the nuclei of IFMs and leg muscles, whereas Hb-GFP is only found in leg muscle nuclei (**H**) and not detectable in IFM nuclei (**D**). Scale bars indicate 5 µm.

Figure 6 -figure supplement 3: Alternative splicing into alternative C-termini

Antibody stainings of the adult thorax with anti-GFP antibody (green or white in the single colour images) and phalloidin (red). (**A, H**) Gene models of the 3' end of *Mhc* (**A**) and *rhea* (**H**) listing the predicted isoforms; coding exons are shown in pink, 3'-UTRs in yellow boxes. The positions of the GFP tag insertions are marked by green arrows. (**B - G**) The shorter Mhc-GFP isoforms (Iso K, L, M) are expressed in IFMs and all leg muscles (**B - D**), whereas the slightly longer Mhc-GFP isoforms (Iso A, F, G etc.) are not detectable in IFMs but present in visceral muscles and a subset of leg muscles (**E - G**). (**I - N**) The shorter Talin-GFP isoforms (*rhea* Iso C, D) are not detectable at muscle-tendon attachment sites in IFMs (**J**, arrowheads) and leg muscles (**K**, arrowhead), however do localise to costamers of leg muscles (**K**). However, the long Talin-GFP isoforms (*rhea* Iso B, E, F, G) do localise to muscle-tendon attachment sites in IFMs (**M**) and leg muscles (**N**). Scale bars indicate 100 µm (**B**, **E**, **I**, **L**), 10µm (**G**) and 5 µm (**C**, **D**, **F**, **J**, **K**, **M**, **N**).

Figure 7: Co-localisation of fTRG tagged proteins with endogenous proteins

Antibody stainings of the adult thorax from fTRG or wild-type lines with anti-GFP antibody (green or white in the single colour images) and antibodies against various fly proteins (red). (**A - D**) Co-localisation of LanA-GFP with anti-Laminin antibody stain around the midgut (**A**), of Par6-GFP with anti-Par6 at the apical side of the proventriculus epithelium (**B**) and of Mlp84B-GFP as well as Mhc-GFP with anti-Mlp84B and anti-Mhc antibody stain in leg muscles, respectively (**C**, **D**). (**E - H**) Adult thoraces from wild-type

flies show very similar patterns with the respective antibodies. (**I** - **L**) Adult IFMs showing the co-localisation of Fln-GFP with anti-Fln antibody staining (**I**), Unc-89/Obscurin-GFP with anti-Obscurin antibody staining (**J**), Dlg1-GFP with anti-Dlg1 antibody staining (**K**) and Mhc-GFP with anti Mhc antibody staining (**L**). (**M** - **P**) The same antibodies result in very similar patterns in wild-type IFMs apart from the a sharp versus a diffuse Mhc pattern comparing wild-type to Mhc-GFP flies (**L**, **P**). (**Q**) Western blots loaded with total protein extract from wild-type, Mlp84B-GFP, Fln-GFP and Dlg1-GFP adult males probed with anti-V5 (included in the GFP tag) anti-Mlp84B, anti-Fln and anti-Dlg1 antibodies. Note the about 40 kDa size shift of the tagged proteins in the respective lanes (marked with green arrow heads) versus the untagged protein band (black arrow heads).

Figure 8: Live imaging of fTRG tagged proteins in living pupal thorax

(**A**) Schematic drawing of a 10 - 12 h (left) and a 30h pupal thorax (right). The developing epidermis is shown in blue, with the SOP precursors in yellow (developing neurons in red), the differentiating tendons are shown in orange, the myoblasts and muscle fibers in green, and the muscle-tendon junction in red. The schematic positions of the optical sections through epithelium and muscles are indicated with blue and green dotted lines, respectively. (**B** - **Y**) Live imaging of pupal thoraces at the indicated stages acquired with a spinning disc confocal (except **S** and **T**, which were acquired with a two-photon microscope). Blue bars above the image indicate epithelial sections and green bars indicate muscle sections (as explained in **A**). Hts-GFP is expressed in fusing myoblasts (**B**, **C**) and strongly in developing SOPs (**D**, **E**). Dlg1-GFP labels the epithelial junctions (**F**), internal muscle structures (green dots, **G**) and an unidentified additional developing epithelium (yellow dots, **H**, **I**). Talin-GFP is higher expressed in developing SOPs (**J**, **K**) and strongly localised to the muscle-tendon junction from 24h APF (red arrowheads, **L**, **M**). LanB1-

GFP localises to the basal side of the developing epithelium (**N**) and surrounds the forming muscle fibers (green dots, **O - Q**) with a slight concentration at the muscle-tendon junction at 30h APF (red arrowheads, **Q**). Act88F-GFP weakly labels the developing epithelium, with a slight concentration in the SOPs until 20h APF (**R**, **S**) and very strongly marks the IFMs from 24h onwards (**T**, **U**). βTub60D-GFPis expressed in the fusing myoblasts (**V**, **W**) and also labels the microtubule bundles in the developing muscle fibers (**X**, **Y**) and hair cells of the developing sensory organs (light blue arrow heads in **X**). Scale bars indicate 10 µm.

Figure 8 -figure supplement 1: Live imaging during pupal development

(**A - F**) Stills from live two-photon imaging of an intact 14h APF pupa expressing Act88F-GFP strongly labelling the developing IFMs (see **Video 4**). (**G - K**) Stills from a two-colour spinning disc Video expressing Act88F-GFP (green) and *him*-GAL4, UAS-palm-Cherry (red) labelling the myoblasts (see **Video 5**). Note the sudden green label of single myoblasts after fusion had occurred (yellow arrowheads, see **Video 5**). (**L - Q**) Stills from two-photon Video of an intact 14h APF pupa expressing βTub-60D-GFP in fusing myoblasts and developing myofibers (See **Video 6**). (**R - V**) Still from a high resolution two-photon Video of an intact 16h APF pupa expressing βTub-60D-GFP. Single myoblast during fusion can be resolved (See **Video 7**). Strong microtubule bundles (red arrow heads) are visible close to the edges of the splitting myotube (white dashed lines, **R**); splitting is complete in (**V**). Scale bars indicate 50 µm (**A - F**, **L - Q**) and 10 µm (**G - K**) and (**R - V**).

Figure 9: Proteomics with fTRG bait proteins

GFP-tagged Ilk, Dlg1, Talin, and LanB1, respectively, were affinity-enriched from protein extracts generated from whole pupae (left) or adult flies (right) using anti-GFP

immunoprecipitation. A wild-type fly strain not expressing any GFP-tagged protein served as control. Proteins were quantified using mass spectrometry and the MaxLFQ label-free quantification algorithm in MaxQuant. Selected proteins are visualized by their enrichment factors in individual samples over the control (or simulated noise level, if not detected in the control). Specific interaction partners are characterised by the similarity of the quantitative profiles and co-enrichment with the respective bait proteins

Table 1: TransgeneOme constructs and fTRG lines - overview

Overview of TransgeneOme constructs generated and verified by sequencing for the different pilot sets and the genome-wide set, including the respective numbers of the transgenic fTRG lines generated.

Table 2: Genetic rescue of mutants with the fTRG lines

Table listing fTRG lines and respective genetic alleles as well as rescue assays that were used to assess the functionality of the fTRG lines. Note that about two-thirds of the lines fully rescue the mutant phenotypes (marked green).

Table 3: *in toto* SPIM imaging of fTRG lines in the embryo

Table listing the fTRG lines that were imaged in the embryo using Zeiss Lightsheet Z.1 from multiple angles over time. *nrv2, gsb* and *gsb-n* are discussed in the text. For the remaining lines we list broad categorisation of the expression detected by SPIM imaging.

Table 4: Summary of adult muscle fTRG expression patterns

54 detected adult muscle localisation patterns (flight muscle, leg muscle and visceral muscle) from Supplementary File 4 are summarised. fTRG line number is listed in brackets.

Supplementary File 1: TransgeneOme constructs

Construct and clone names, tag locations, as well the sequencing validation data are listed for all TransgeneOme constructs generated. Sheet 1 lists the sGFP TransgeneOme (TY1-sGFP-V5-BLRP-FLAG tag, NGS sequenced), sheet 2 the TY1-sGFP-FLAG pilot set clones (junctions Sanger sequenced, only exact matches are counted as verified), sheet 3 the TY1-T2A-sGFPnls-FLAG pilot set clones (entire tag Sanger sequenced) and sheet 4 the TY1-sGFP-V5-BLRP-FLAG pilot set clones (entire tag Sanger sequenced). Sheet 5 summarises all verified tagged genes in these sets.

Supplementary File 2: fly TransgeneOme lines (fTRG) lines

Table listing all 880 transgenic FlyFos (fTRG) lines, with fTRG numbers, construct and clones names, as well as nature of the tag and the used landing site. The second sheet compares the genes tagged by the fTRG lines to the available GFP gene trap lines. 765 genes are only found in the TransgeneOme resource.

Supplementary File 3: fTRG expression in ovaries

Table listing the expression patterns for 115 fTRG lines in ovaries. Expression was detected in 94 lines by anti-GFP antibody stainings. Cell type specific expression and subcellular localisations were monitored for these lines.

Supplementary File 4: fTRG expression in the adult thorax

Table listing the expression pattern for 121 fTRG lines in adult thoraces. Expression was detected in 101 lines by anti-GFP antibody stainings. Cell type specific expression and subcellular localisations were monitored for these lines.

Supplementary File 5: Proteomics quantification

Quantitative mass spectrometry values of all detected protein obtained with the MaxQuant software suite for all the GFP-enrichment experiments are listed.

Video 1

Multi-view SPIM Video of a stage 12 Nrv2-GFP expressing embryo. A stack was acquired every 15 minutes, lateral, dorsal, ventral and transverse views of the same time points are displayed. From stage 11 onwards Nrv2-GFP is present ubiquitously in the plasma membrane. Later its expression increases in the CNS, particularly in the neuropil and the motor neurons. Video plays with 7 frames per second. Time is given in hh:mm. Scale bar indicates 50 µm.

Video 2

Lateral head section from a SPIM Video of a stage 10 Gsb-GFP (green, white in the top Video), Histone-2A-mRFPruby (red) embryo. A stack was acquired every 7 minutes. The segmentally re-iterated stripe-like *gsb* expression domain in the head neuroectoderm is visible. Later, *gsb* is expressed in ganglion mother cells and nerve cells that are the progeny of *gsb* expressing neuroblasts. Video plays with 7 frames per second. Time is given in hh:mm. Scale bar indicates 50 µm.

Video 3

Ventral view of a SPIM Video of a stage 6 Gsb-n-GFP embryo. A stack was acquired every 15 minutes. Gsb-n-GFP is only detectable at the end of germ-band extension. During germ-band retraction it is expressed in characteristic L-shaped expression domains in the hemi-segments of the trunk. In the late stage embryo Gsb-n-GFP is present in the neurons of the shortening ventral nerve cord. Video plays with 7 frames per second. Time is given in hh:mm. Scale bar indicates 50 μm.

Video 4

Z-projection of a two-photon Video of an about 14h APF pupa expressing Act88F-GFP. A stack was acquired every 20 min for 19 h. Expression of Act88F-GFP increases in the indirect flight muscles dramatically, thus contrast was reduced several times in course of the Video to avoid over-exposure. Video plays with 5 frames per second. Time is given in hh:mm.

Video 5

Single plane of a spinning disc confocal Video of an about 14 h APF old pupa expressing Act88F-GFP (green) in the flight muscle myotubes and *him*-GAL4; UAS-palm-Cherry in the myoblasts. An image stack was acquired every two minutes. Note the newly fused myoblasts acquired the GFP label within a single time interval (highlighted by green arrows). Video plays with 5 frames per second. Time is given in minutes.

Video 6

Z-projection of a two-photon Video of an about 14h APF pupa expressing βTub60D-GFP. A stack was acquired every 20 min for 25 h. Note the high expression of βTub60D-GFP in fusing myoblasts and the thick microtubules bundles in the developing flight muscles. Hair

cells of the developing sensory organs also show strong expression, however move out of the Z-stack over time. Video plays with 5 frames per second. Time is given in hh:mm.

Video 7

Single plane of a two-photon Video of an about 16 h APF old pupa expressing βTub60D-GFP in myoblasts and the forming flight muscle myotubes. An image stack was acquired every two minutes for more than 3 h. Note that single myoblasts can be followed during fusion. Most myoblasts fuse in the center of the myotube, which gradually splits into two myotubes. Video plays with 5 frames per second. Time is given in hh:mm.

Tagged constructs and transgenic lines

	constructs	verified constructs	transgenic lines
'pre-tagging' - TransgeneOme	11257	--	--
TY1-sGFP-V5-BLRP-FLAG			799
- TransgeneOme	10995	9580	
- pilot set	1328	1328	
TY1-T2A-sGFPnls-FLAG			
- pilot set	273	273	30
TY1-sGFP-FLAG			
- pilot set	644	483	51
unique constructs	**23169**	**10711**	**880**
unique genes	**11257**	**9993**	**826**

Sarov et al. Table 1

1686

1687

1688

Genetic rescue of mutants with the fTRG lines

Gene	Chromo-some	fTRG line	Tag	Rescue?	Rescue assay	Alleles, deficiencies used in trans for rescue assay	Reference
amos	2nd	**fTRG_218**	2xTY1-sGFP-V5-preTEV-BLRP-3xFLAG	**yes**	antenna size and bristle number rescued to normal	*amos[3]*	
anterior open (aop, Yan)	2nd	**fTRG_142**	2xTY1-sGFP-V5-preTEV-BLRP-3xFLAG	**yes**	embryonic lethality rescued to viable adults	*aop[1]* (BL-3101); *aop[Yan1]* (BL-8780)	
aubergine (aub)	2nd	**fTRG_581**	2xTY1-sGFP-V5-preTEV-BLRP-3XFLAG	**yes**	female sterility entirely rescued	*aub[HN2*] (BL-8517); Df(2L)BSC145 (BL-9505)	
baboon (babo)	2nd	**fTRG_444**	2xTY1-sGFP-V5-preTEV-BLRP-3xFLAG	**yes**	lethality rescued to viable adults	*babo[32]* (BL-5399); *babo[k16912]* (BL-11207)	
bag of marbles (bam)	3rd	**fTRG_3**	2xTY1-sGFP-V5-preTEV-BLRP-3xFLAG	**yes**	female sterility entirely rescued	*bam[delta86]; Df(3R)exel9020*	Christian Bökel, pers. comm.
cactus (cact)	2nd	**fTRG_516**	2xTY1-sGFP-V5-preTEV-BLRP-3xFLAG	**yes**	lethality and female sterility rescued	*cact[1]; cact[4]*	
CG32121	3rd	**fTRG_92**	2xTY1-sGFP-V5-preTEV-BLRP-3xFLAG	**yes**	flightlessness rescued	*CG32121[XZ1]* (X. Zhang and F.S., unpublished); Df(3L)ED4502 (BL-8097)	
CG6509 (dlg5)	2nd	**fTRG_10251**	2xTY1-sGFP-3xFLAG	**yes**	lethality rescued to viable adults	*CG6509[KG006748]* (BL13692); Df(2L)BSC244 (BL-9718)	
discs large 1 (dlg1)	X	**fTRG_502**	2xTY1-sGFP-V5-preTEV-BLRP-3xFLAG	**yes**	male lethality rescued to viable adults	*Dlg1[5]* (BL-36280)	
dorsal (dl)	2nd	**fTRG_29**	2xTY1-sGFP-V5-preTEV-BLRP-3xFLAG	**yes**	bristle number rescued to normal	*dl[1]; dl[4]*	
ebi	2nd	**fTRG_10141**	2xTY1-sGFP-3xFLAG	**yes**	lethality rescued to viable adults	*ebi[CCS-8]* (BL-8397); *ebi[E90]* (BL-30720)	
escargot (esg)	2nd	**fTRG_10170**	2xTY1-sGFP-3xFLAG	**no**	lethality not rescued	*esg[35Ce-1]* (BL-3900); *esg[35Ce-3]* (BL-30475)	
eyes absent (eya)	2nd	**fTRG_492**	2xTY1-sGFP-V5-preTEV-BLRP-3XFLAG	**no**	lethality not rescued	*eya[C0233]; eya[C0275]*	
fat (ft)	2nd	**fTRG_10233**	2xTY1-T2A-nlsGFP-3xFLAG	**yes**	lethality rescued to viable adults	*ft[G-rv]* (BL-1894); *ft[8]* (BL-5406)	
48 related 2 (Fer2)	3rd	**fTRG_334**	2xTY1-sGFP-V5-preTEV-BLRP-3XFLAG	**yes**	defective climbing rescued to wild type	*Fer2[e03248]*	Bou Dib *et al.* 2014
fizzy (fzy)	2nd	**fTRG_10250**	2xTY1-T2A-nlsGFP-3xFLAG	**no**	lethality not rescued	*fzy[1]* (BL-2492); *fzy[3]* (BL-25143)	
flightless I (flil)	X	**fTRG_467**	2xTY1-sGFP-V5-preTEV-BLRP-3xFLAG	**yes**	lethality or flightlessness rescued	*fli[14]* (BL-7481); *fli[3]* (BL-4730)	
Hand	2nd	**fTRG_10163**	2xTY1-sGFP-3xFLAG	**yes**	lethality rescued to viable adults	*Hand[173]*	
hippo (hpo)	2nd	**fTRG_10130**	2xTY1-sGFP-3xFLAG	**yes**	larval lethality rescued to viable adults	*hpo[KS240]* (BL-25085); *hpo[KC202]* (BL-25090)	
HLH54F	2nd	**fTRG_153**	2xTY1-sGFP-V5-preTEV-BLRP-3xFLAG	**yes**	lethality rescued to viable adults	*bHLH54F[598];* Df(2R)Exel7150 (BL-7891)	
Integrin linked kinase (Ilk)	3rd	**fTRG_483**	2xTY1-sGFP-V5-preTEV-BLRP-3xFLAG	**yes**	embryonic lethality rescued to viable adults (wing blisters)	*Ilk[1]* (BL-4861) ; *Df(3L)BSC733* (BL-26831)	
Kinesin heavy chain (Khc)	2nd	**fTRG_10243**	2xTY1-T2A-nlsGFP-3xFLAG	**yes**	lethality rescued to viable adults	*Khc[8]* (BL-1607); *Khc[1ts]* (BL-31994)	
LanB1	2nd	**fTRG_681**	2xTY1-sGFP-V5-preTEV-BLRP-3XFLAG	**yes**	lethality rescued to viable adults	*LanB1[KG03456]* (BL-13957)*; Df(2L)Exel7032* (BL-7806)	

multiple ankyrin repeats single KH domain (mask)	3rd	**fTRG_486**	2xTY1-sGFP-V5-preTEV-BLRP-3xFLAG	**yes**	lethality rescued to viable adults	*mask[10.22]/Df(3R)BSC317*	Barry Thompson, pers. comm
midline (mid)	2nd	**fTRG_490**	2xTY1-sGFP-V5-preTEV-BLRP-3xFLAG	**no**	lethality not rescued	*mid[B1295]*; *mid[C2372]*	
numb	2nd	**fTRG_25**	2xTY1-sGFP-V5-preTEV-BLRP-3xFLAG	**yes**	lethality rescued to viable adults	*numb[1]* (BL-4096); Df(2L)30A-C(BL-3702)	
odd skipped (odd)	2nd	**fTRG_47**	2xTY1-sGFP-V5-preTEV-BLRP-3xFLAG	**no**	lethality not rescued	*odd[5]* (BL-5345); Df(2L)Exel7018 (BL-7789)	
optomotor-blind-related-gene-1 (org-1)	X	**fTRG_485**	2xTY1-sGFP-V5-preTEV-BLRP-3xFLAG	**no**	male lethality not rescued	*org-1[OJ487]*	
oskar (osk)	3rd	**fTRG_1394**	2XTY1-SGFP-V5-preTEV-BLRP-3XFLAG	**yes**	female sterility entirely rescued	*osk[A87]/Df(3R)p-XT103*	
Pabp2	2nd	**fTRG_565**	2xTY1-sGFP-V5-preTEV-BLRP-3XFLAG	**no**	lethality not rescued	*Pabp2[01]* (BL-9838); *Pabp2[55]* (BL-38390)	
patched (ptc)	2nd	**fTRG_82**	2xTY1-sGFP-V5-preTEV-BLRP-3xFLAG	**yes**	lethality rescued to viable adults	*ptc[9]* (BL-3377); *ptc[16]* (BL-35500)	
retina abarrent in pattern (rap)	X	**fTRG_1253**	2xTY1-sGFP-V5-preTEV-BLRP-3XFLAG	**yes**	lethality rescued to viable adults	*rap[ie28]*	Yuu Kimata, pers. comm.
rhea (Talin)	3rd	**fTRG_587**	2xTY1-sGFP-V5-preTEV-BLRP-3XFLAG	**yes**	embryonic lethality rescued to viable adults	*rhea[1]* ; *rhea[79]*	
RhoGEF2	2nd	**fTRG_591**	2xTY1-sGFP-V5-preTEV-BLRP-3XFLAG	**yes**	embryonic lethality rescued to viable adults	*RhoGEF2[04291]*	Jörg Großhans, pers. comm.
roundabout (robo)	2nd	**fTRG_567**	2xTY1-sGFP-V5-preTEV-BLRP-3XFLAG	**no**	lethality not rescued	*robo[1]* (BL-8755); *robo[2]* (BL-8756)	
saxophone (sax)	2nd	**fTRG_10070**	2xTY1-sGFP-3xFLAG	**yes**	lethality rescued to viable adults	*sax[4]* (BL-5404); *sax[5]* (BL-8785)	
scribbler (sbb)	2nd	**fTRG_443**	2xTY1-sGFP-V5-preTEV-BLRP-3xFLAG	**no**	lethality not rescued	*sbb[04440]* (BL-11376); Df(2R)BSC334 (BL-24358)	
Sin3A	2nd	**fTRG_596**	2xTY1-sGFP-V5-preTEV-BLRP-3XFLAG	**no**	lethality not rescued	*Sin3A[08269]* (BL-12350); *Sin3A [B0948]*	
smoothened (smo)	2nd	**fTRG_599**	2xTY1-sGFP-V5-preTEV-BLRP-3XFLAG	**yes**	lethality rescued to viable adults	*smo[3]* (BL-3277); *smo[119B6]* (BL-24772)	
snail (sna)	2nd	**fTRG_71**	2xTY1-sGFP-V5-preTEV-BLRP-3xFLAG	**no**	lethality not rescued	*sna[18]* (BL-2311); *sna[1]* (BL-25127)	
spalt major (salm)	2nd	**fTRG_165**	2xTY1-sGFP-V5-preTEV-BLRP-3xFLAG	**no**	lethality not rescued	*salm[1]* (BL-3274); Df(2L)32FP-5 (BL-29717)	
Target of rapamycin (Tor)	2nd	**fTRG_713**	2xTY1-sGFP-V5-preTEV-BLRP-3XFLAG	**no**	lethality not rescued	*Tor[deltaP]* (BL-7014); Df(2L)Exel7055 (BL-7823)	
traffic jam (tj)	2nd	**fTRG_163**	2xTY1-sGFP-V5-preTEV-BLRP-3xFLAG	**no**	sterility not rescued	*tj[PL3]* (BL-4987); Df(2L)Exel8041 (BL-7849)	
viking (vkg)	2nd	**fTRG_595**	2xTY1-sGFP-V5-preTEV-BLRP-3XFLAG	**no**	lethality not rescued	*vkg[01209]* (BL-11003); Df(2L)Exel7022 (BL-7794)	
Unc-89/ Obscurin	2nd	**fTRG_1046**	2xTY1-sGFP-V5-preTEV-BLRP-3XFLAG	**yes**	flightlessness rescued	*Unc-89[EY15484]*	
yorkie (yki)	2nd	**fTRG_875**	2xTY1-sGFP-V5-preTEV-BLRP-3XFLAG	**yes**	lethality rescued to viable adults	*yki[B5]*	Barry Thompson, pers. comm.

Sarov et al. Table 2

1689

1690

in toto SPIM imaging of fTRG lines in the embryo

fTRG number	FBgn_id	Gene symbol	Signal	Embryonic expression	Movie	Beads
58	FBgn0001148	***gsb***	strong	tissue specific expression	Yes	Yes
71	FBgn0003448	***snail***	weak	tissue specific expression	Yes	Yes
88	FBgn0025360	***Optix***	medium	tissue specific expression	Yes	Yes
94	FBgn0010433	***ato***	weak	tissue specific expression	Yes	Yes
137	FBgn0259685	***crb***	medium	tissue specific expression	Yes	Yes
155	FBgn0029123	***SoxN***	strong	tissue specific expression	Yes	Yes
349	FBgn0024294	***spn43Aa***	strong	late expression, deposited in the cuticle	Yes	Yes
513	FBgn0001147	***gsb-n***	medium	tissue specific expression	Yes	Yes
937	FBgn0015777	***nrv2***	strong	ubiquitous expression, membrane signal	Yes	Yes

Sarov et al. Table 3

1694

Summary of adult muscle fTRG expression patterns

thick filament	thin filament / myofibril	M-line	Z-disc	muscle attachment site	T-tubules / sarcolemma	dotty pattern / vesicles (?)	mito-chondria	nucleus	neuro-muscular junction
Fln (876, IFM)	Act88F (78, 10028, IFM)	Prm (475, IFM)	CG31772 (63)	Ilk (483)	Dlg1(502)	Babo (444)	CG12118 (276)	Adar (570)	Cact (516)
Mf (Iso-A,G, N, 501)	Fray (125, 10032)	Unc-89 (1046)	Kettin (Sls-Isoform, 569)	Talin (*rhea*, Iso-B, E, F, G, 587)	Sax (10070)	CG5885 (10017, leg m.)		Blimp-1 (10149)	Veli (10125)
Mhc (Iso-K, L, M, 500)	Hsp83 (10010)		Lmpt (584, I-band, leg m.)	β-PS Integrin (*mys*, 932)		CLIP-190 (156)		CG11617 (10041)	
Mhc (Iso-A, F, 519, leg m. subset & visceral. m.)	TpnC25D (1257, leg m. & visceral m.)		Mask (486, IFM)			Dlg5 (*CG6509*, 10251, IFM)		CG12391 (10036)	
Prm (475, leg m. & visceral m.)	TpnI (*wupA*, 925, leg m. & visceral m.)		Mlp60A (709, leg m. & visceral m.)			Hts (585)		CG17912 (10035)	
			Mlp84B (678, leg m. & visceral m.)			Mask (486, leg m.)		CG32121 (92)	
			Talin (Iso-C, D, 731, leg m. & visceral m.)			Pyd3 (53)		Dorsal (29, leg m.)	
						Rho1 (31)		E2F2 (115)	
						Sc2 (79, 10039)		Gro (21)	
						Tango11 (699)		Hand (10163, visceral m.)	
						Tsc1 (59)		Hb (139, leg m.)	
						Vps35 (*CG5625*, 57)		Mnt (34)	
								P53 (84)	
								Salm (165)	
								Vri (182)	

Sarov et al. Table 4

1695

1696

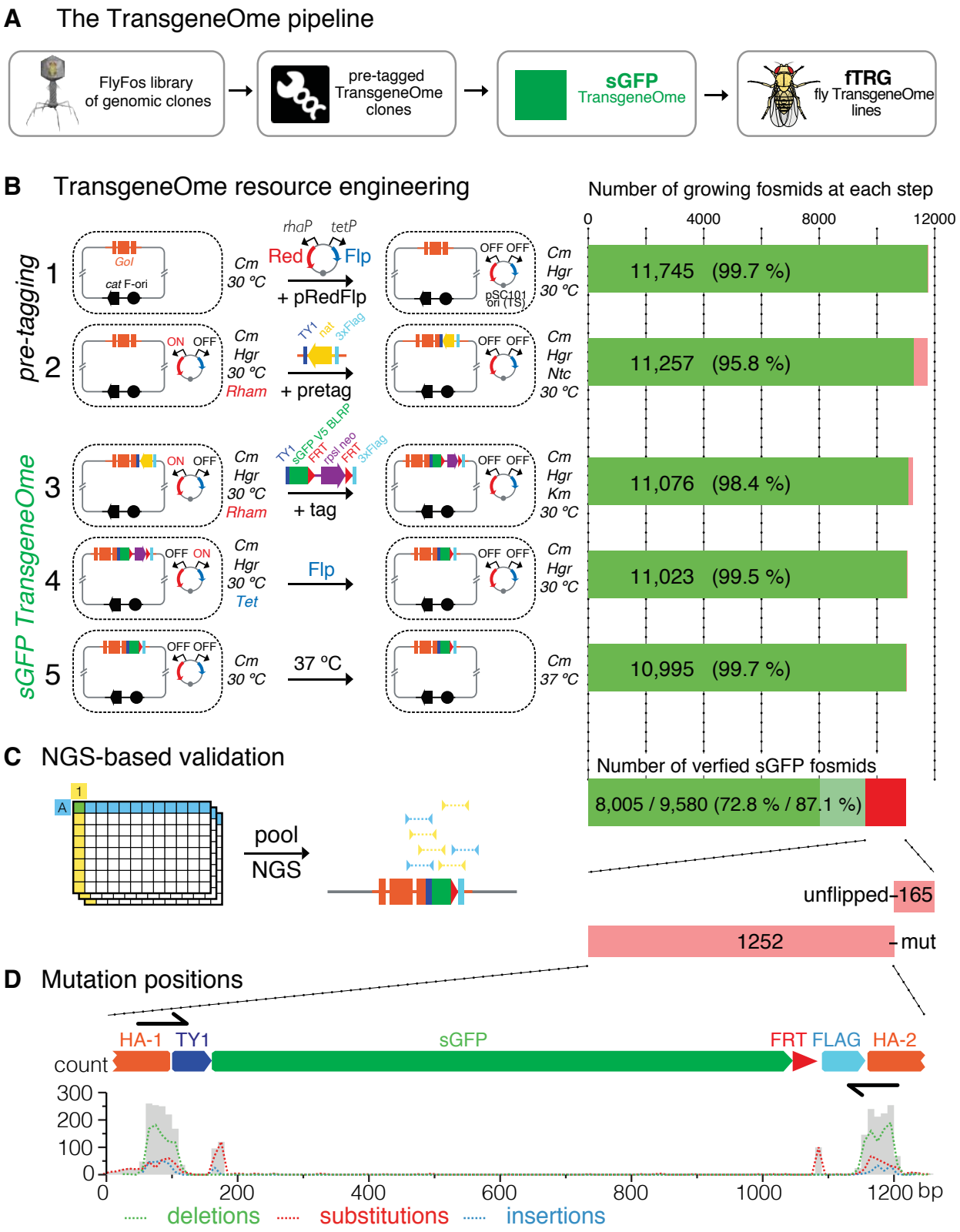

Sarov et al. Figure 1

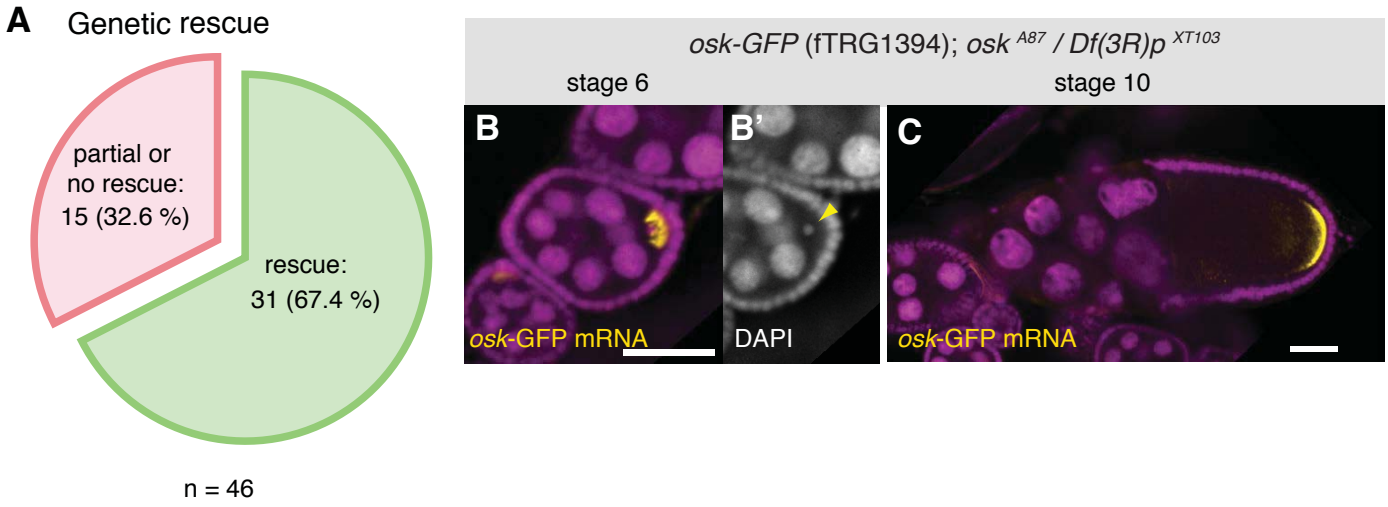

Sarov et al. Figure 2

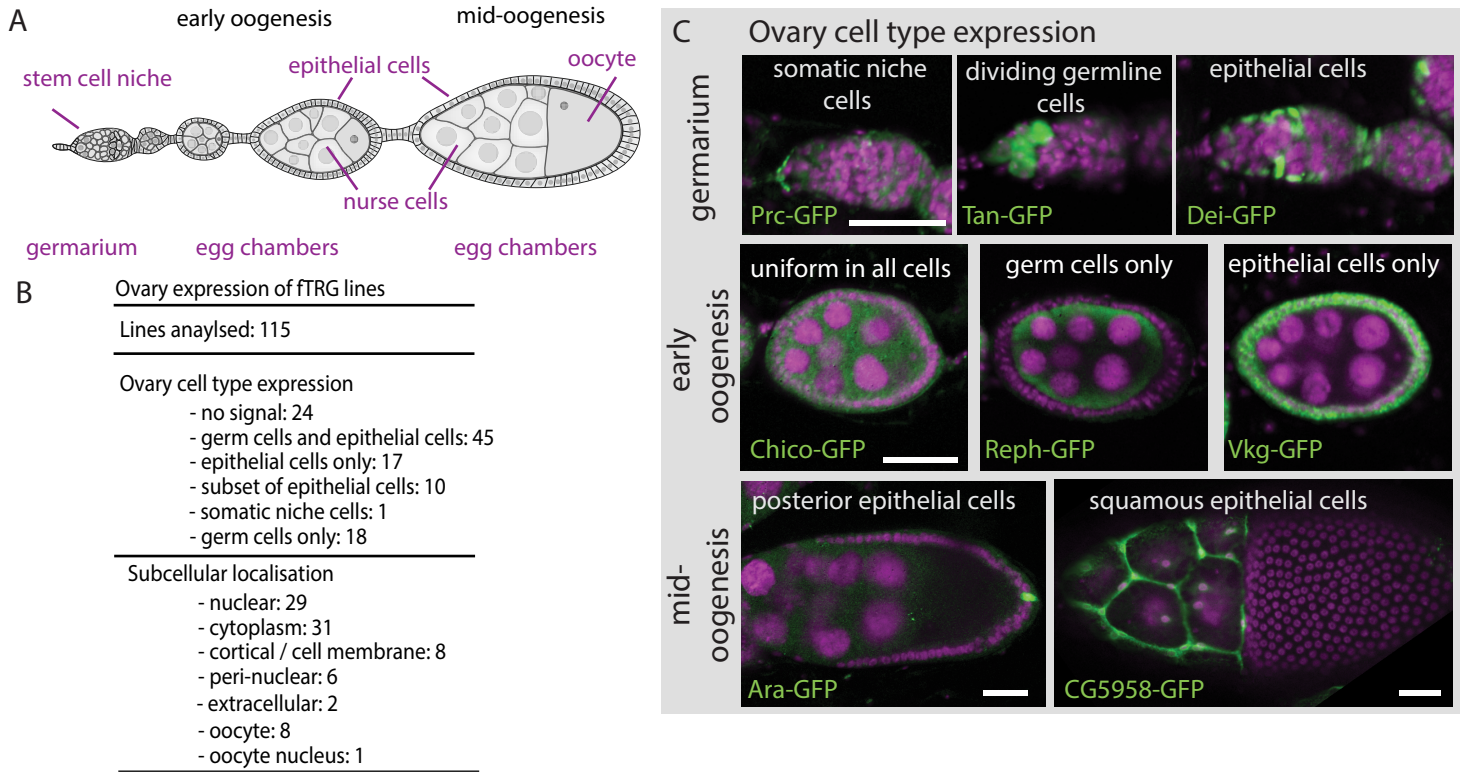

Sarov et al. Figure 3

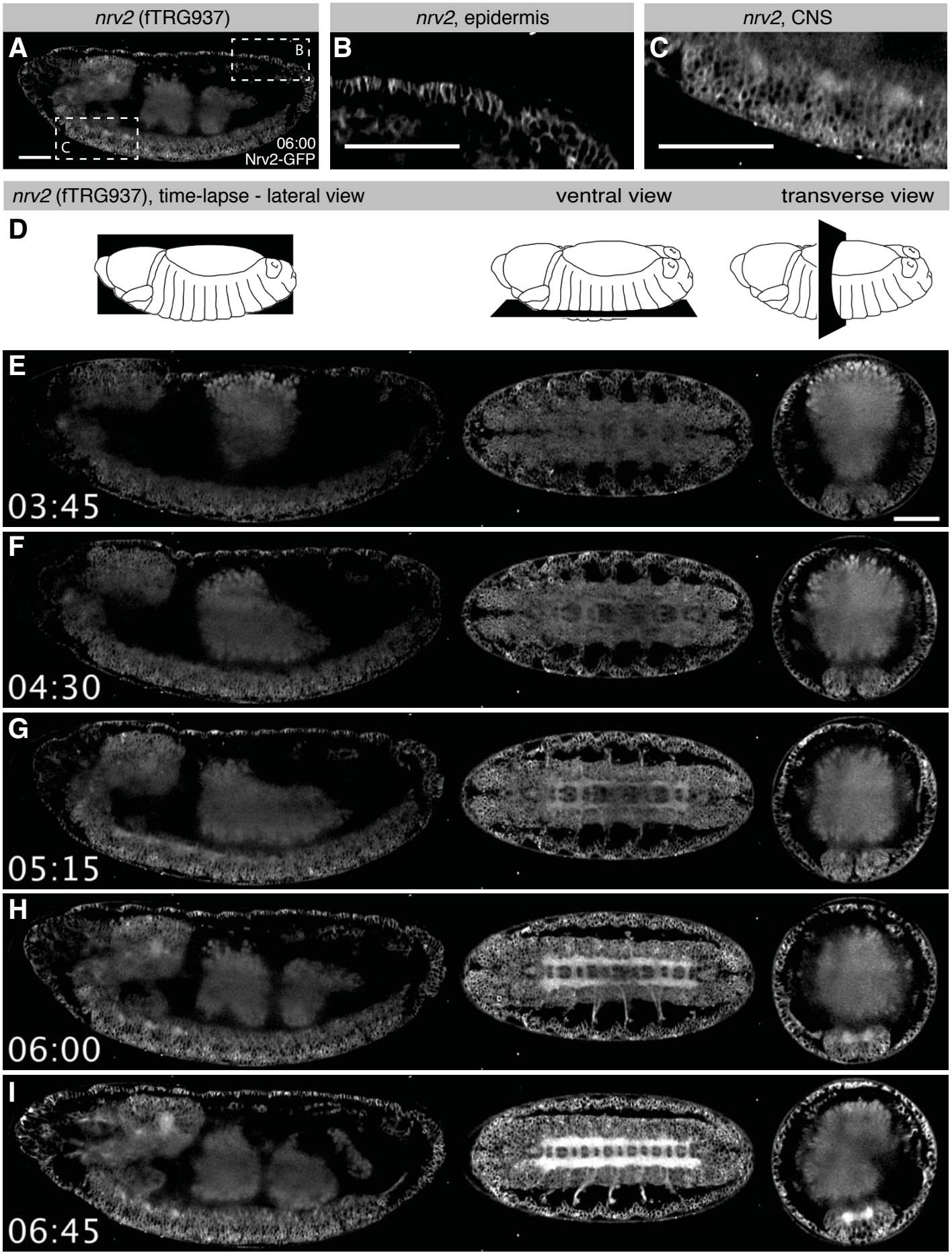

Sarov et al. Figure 4

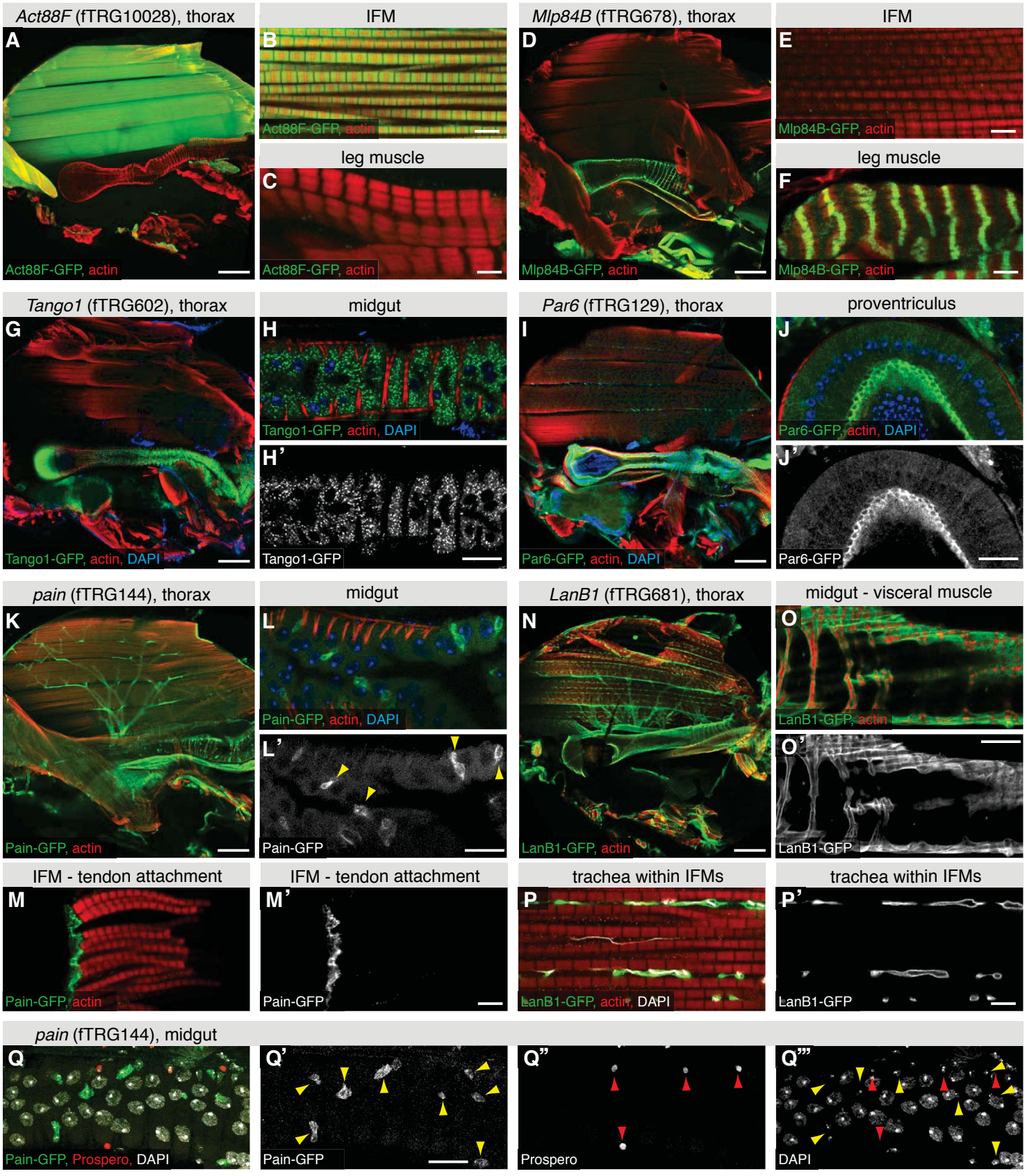

Sarov et al. Figure 5

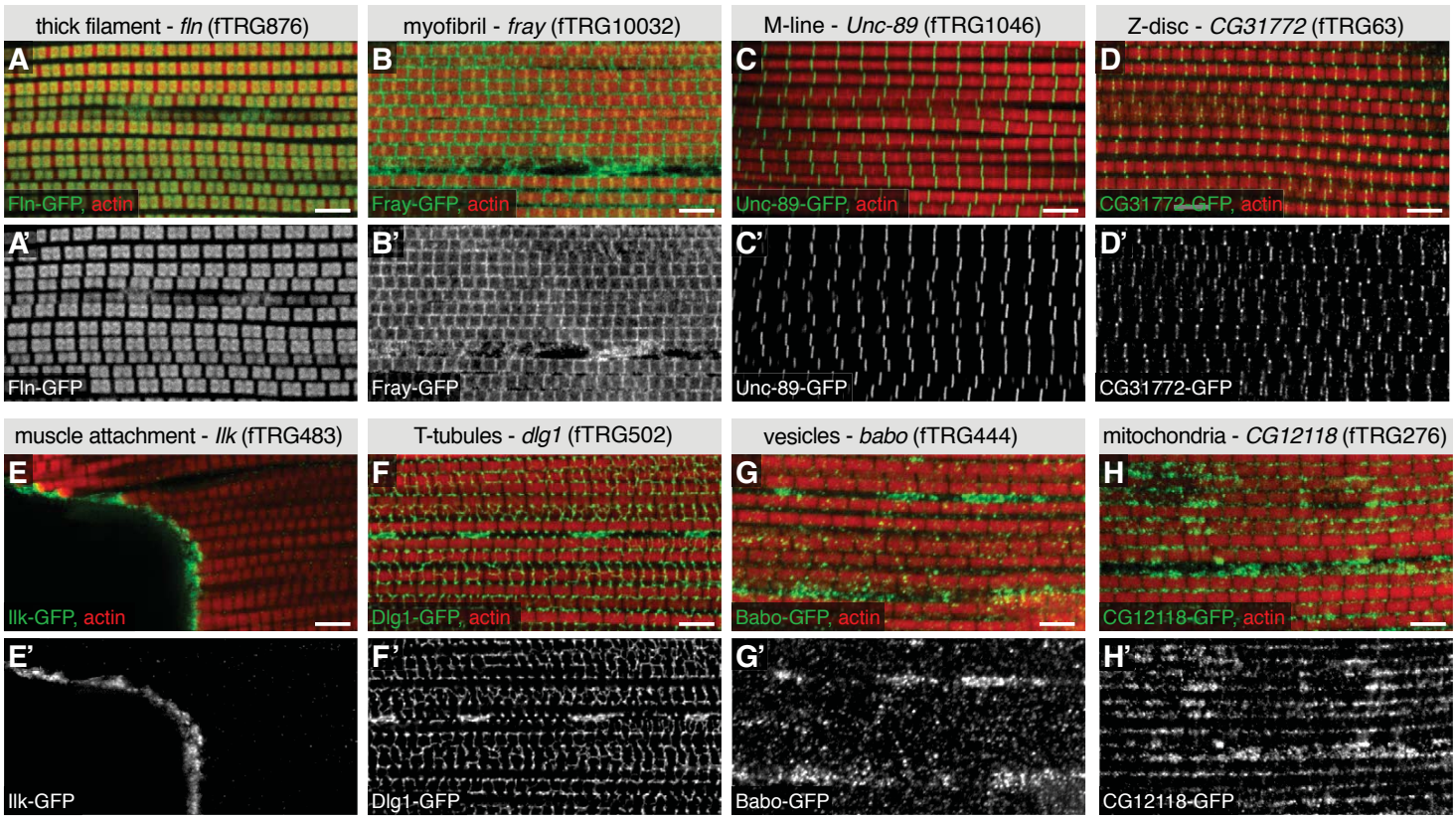

Sarov et al. Figure 6

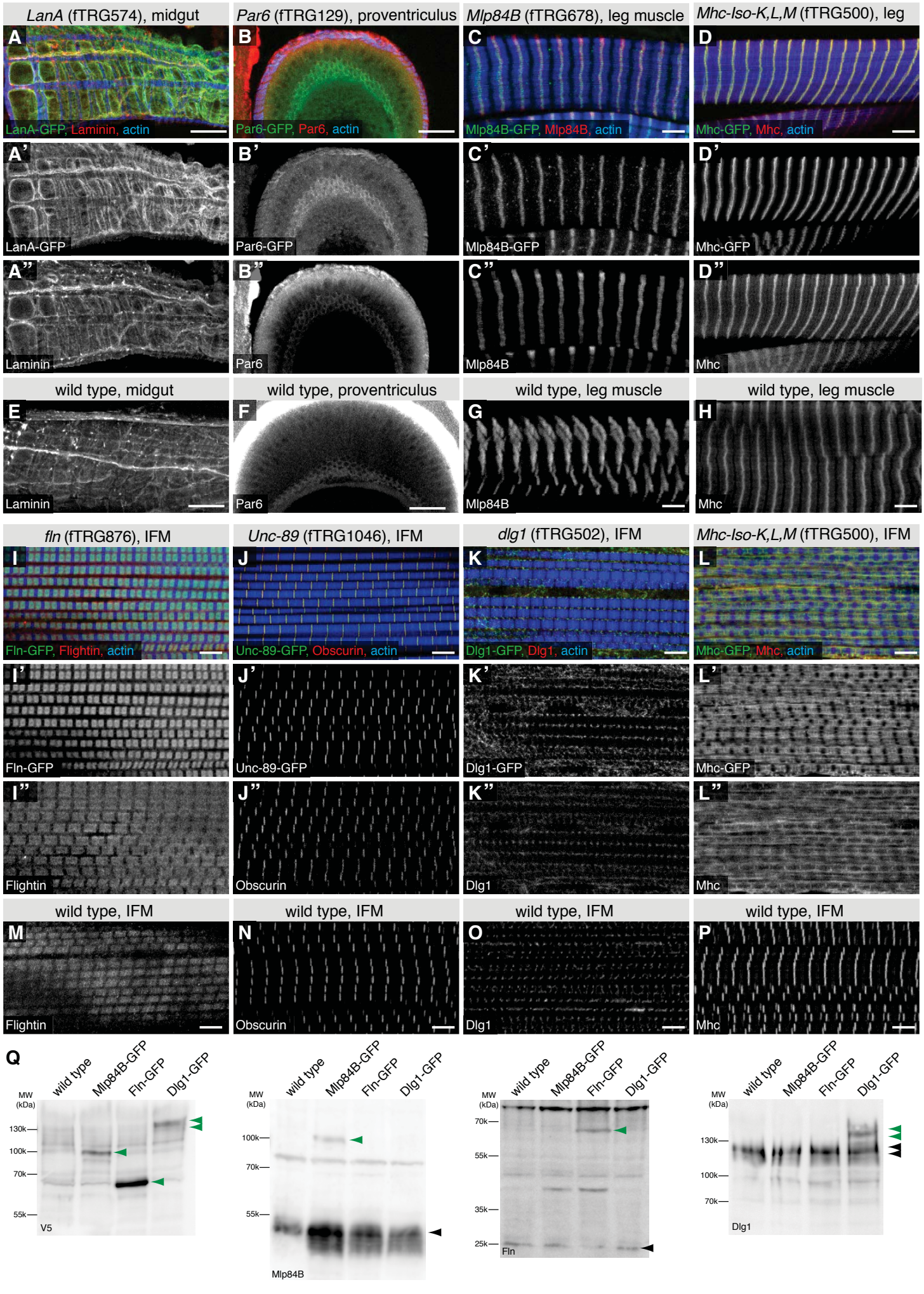

Sarov et al. Figure 7

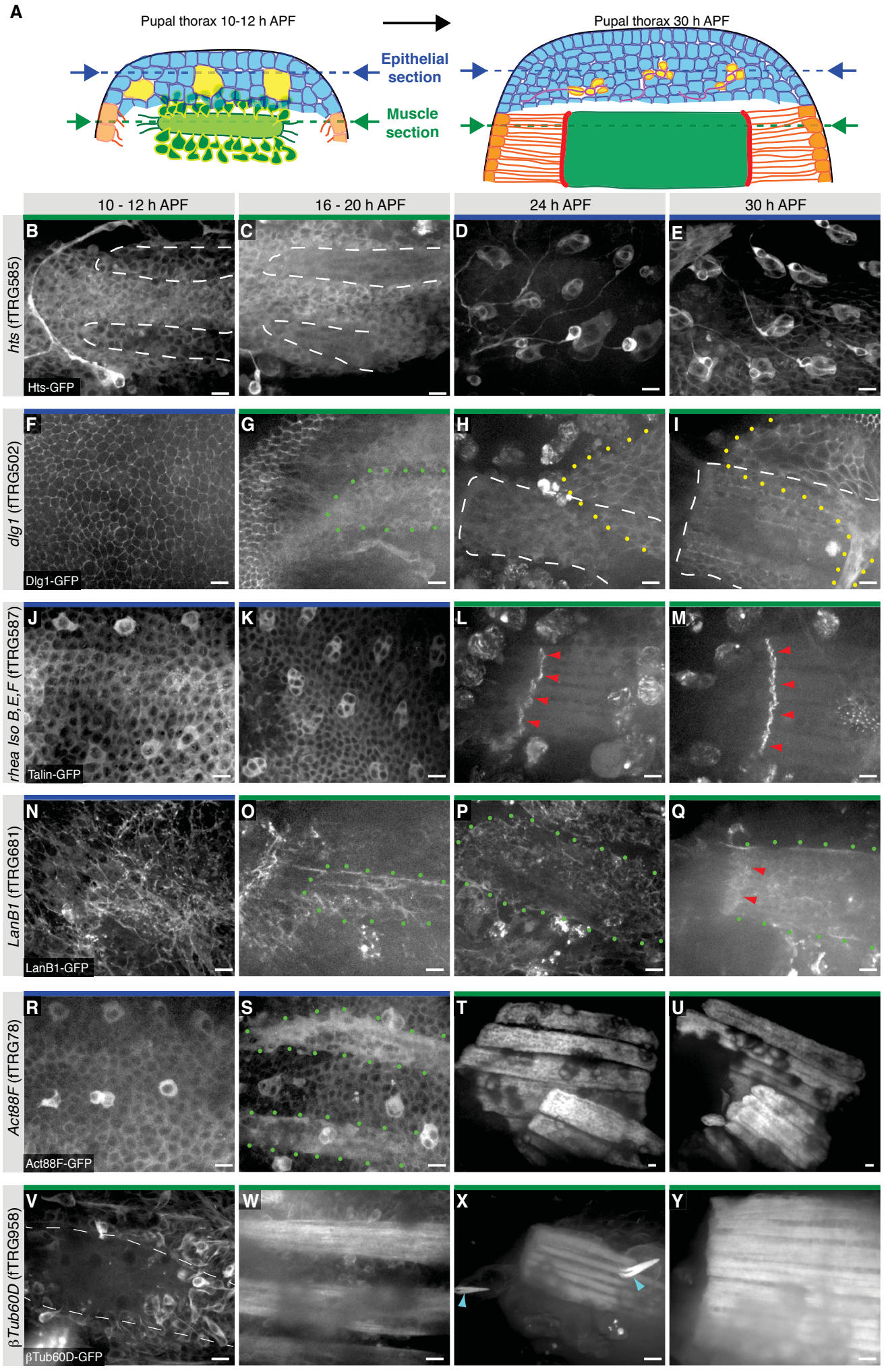

Sarov et al. Figure 8

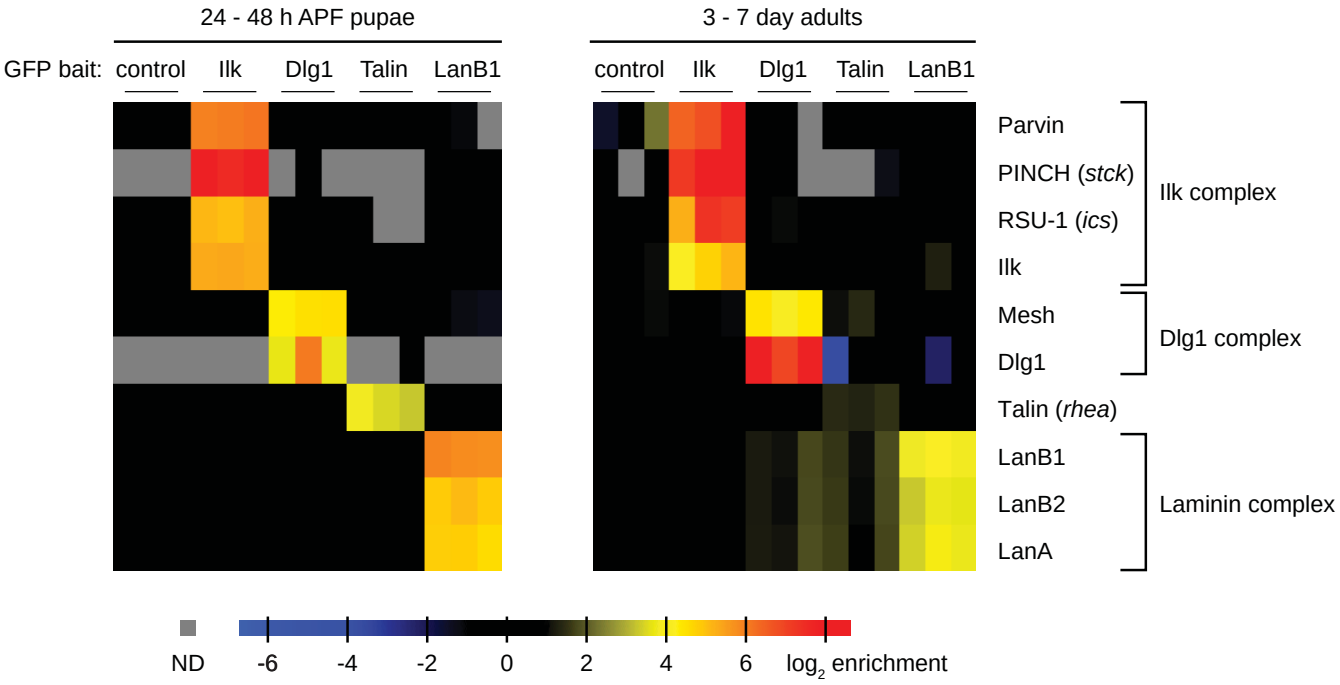

Sarov et al. Figure 9